

Physical properties of the environment relevant to the pelagic ecosystem of a deep high-mountain lake (Estany Redó, Central Pyrenees)

JORDI CATALÁN

Departament d'Ecologia. Facultat de Biologia. Universitat de Barcelona. Diagonal, 645. 08028 Barcelona

Recibido: sSetiembre 1988.

RESUMEN

El medio físico relacionado con el ecosistema pelágico de un lago profundo de alta montaña (Estany Redó, Pirineos centrales). El medio físico de un lago puede caracterizarse fundamentalmente con cuatro descriptores: temperatura, luz, energía cinética turbulenta y la morfología de la cuenca. En este estudio presentamos estas características para el Estany Redó, un lago de alta montaña situado en el Pirineo central y originado por la acción modeladora de las glaciaciones del Pleistoceno. El lago se encuentra en una cuenca granodiorítica en forma de anfiteatro y de laderas muy pendientes. El suelo y la vegetación están poco desarrollados en toda la cuenca. El lago es profundo (73 m) en relación a su área (24 hm²), y su volumen (7.75 hm³) es considerable en relación a su cuenca de recepción (155 hm²). En los lagos de sus dimensiones (longitud mínima 655 m), la fuerza del viento sólo tiene un papel distribuidor de sedimento en un estrecho margen litoral y los procesos de deposición están gobernados por la pendiente. Como en el Redó la pendiente de las paredes es muy acusada el sedimento fino no se deposita de forma estable en las plataformas profundas. El tiempo medio de residencia del agua en el lago es cercano a los cuatro años, que considerado por capas supone unos 2 años para las capas superiores (0-5 m) y más de 15 años para las más profundas (40 m). El lago permanece helado durante medio año, de Diciembre a Junio. En el período que está libre de hielo la radiación solar penetra profundamente debido a la transparencia del agua (disco de Secchi hasta 17 m). En invierno, la acumulación de nieve (2 m) impide el paso de luz. Debido al alto tiempo de residencia del agua, la estructura de la columna de agua está gobernada por los intercambios de calor y la acción del viento. Se trata de un lago dimíctico clásico. La mezcla de primavera es más corta que la de otoño. Después del deshielo, rápidamente se forma una incipiente termoclina entre 3-4 m, que rápidamente se traslada a profundidades mayores (c. 13 m) por la acción del viento. La termoclina permanece estable durante poco más de un mes, mientras el flujo medio de calor es positivo. Cuando el flujo de calor se invierte, la convección debilita y hunde la termoclina rápidamente. Sin embargo, la distinción de dos capas (epi- e hipolimnion) es válida hasta que prácticamente la mezcla llega al fondo del lago. Desde un punto de vista biológico, la pequeñez de la cuenca en relación al volumen del lago favorece una oligotrofia extrema. Por otro lado, la disposición del sedimento fino (importante en el reciclado de nutrientes) a profundidades por debajo de la termoclina estable, favorece una pauta de producción biológica estrechamente relacionada con los períodos de mezcla de la columna. La alta penetración de la luz y la falta de aportes de nutrientes al hipolimnion pueden favorecer la formación de mínimos profundos de clorofila en verano, lejos de las capas fotoinhibidoras superiores. De cualquier modo, la baja temperatura supone en todo momento un límite a la velocidad de los procesos biológicos tanto de producción como de respiración.

SUMMARY

From an ecological approach the physical environment of lakes can be summarized by four components: temperature, light, turbulence and the morphology of the basin and its watershed. The variability through an annual cycle of these components of the physical environment of the Estany Redó is described in the paper and their implications for the dynamics of its biota are examined. The ratio between catchment area size (155 hm²) and lake volumen (7.75 hm³) is extremely small. The value of relative depth is extraordinarily high (13 %). Both aspects contribute to the oligotrophy of the lake. Because of the hypsographic configuration of the lake Redó there is a sediment focusing above 40 m and between 15 and 25 m. Production peaks should be linked to the interaction of the mixing layer with these sediment-rich bottoms. Other implications of the temperature, the light and the mixing time scales in the lake biological dynamics are also examined.

KEYWORDS: Redó, physical limnology, high-mountain lakes, pelagic ecosystems.

PALABRAS CLAVE: Redó, limnología física, lagos de alta montaña, ecosistemas pelágicos.

INTRODUCTION

The physical features of different ecosystems are important determinants of their biological structure and dynamics. Superimposed to the plasticity of the different species and the complexity of the communities, the physical environment sets the main characteristics of production and seasonal changes of the ecosystem. The physical environment of lakes can be summarized by four important components: temperature, light, turbulence and the morphology of the basin and its watershed. These components differ in their temporal variability, with the morphological characteristics being quite stable throughout the year for most lakes, whereas the remaining components are subject to strong seasonal variations. These seasonal variance is enhanced in high mountain lakes, such that they provide great opportunities for the examination of the coupling of physical and biological processes (CATALÁN, 1986). Here we describe the variability throughout an annual cycle of these four components of the physical environment of the Estany Redó (Central Pyrenees) to examine its implications for the dynamics of its biota.

MATERIAL AND METHODS

The lake Redó ($42^{\circ} 3' 33.5''$ N, $0^{\circ} 46' 12.7''$ E) is located in the upper portion of the basin of the Noguera Ribagorça River. Its watershed is delimited to the East by the peak of Port de Vielha (2606 m); to the West by the peak of the Sarraera (2632 m) and the peak of Estany Redó (2540 m); and to the North by the mountain range joining the two largest peaks, that corresponds to the divisory between the Southern and Northern slopes of the axial range of the Pyrenees. The lake effluent discharges towards the South.

Pyrenees lakes originated as a consequence of the morphogenic activity of the Pleistocene glaciations. The basin of

Redó Lake occupies a former glacial cirque that fed the glaciers descending the Valley of Conangles towards the main glacier of the Valley of the Noguera Ribagorça. Although the Pleistocenic glacierism was a multiple process the glacial dynamics acted in the Redó cirque through all the successive pulsations (VILAPLANA, 1983). Since the end of the glacial period the cirque has experienced intense periglacial dynamics, mainly gelifraction, that yielded its current morphometry. We can locate the onset of the lacustrine dynamics described at about 10,000 B.P.

The morphology of the lake was studied following the procedures outlined in HAKANSON (1981), complemented with additional morphometric parameters proposed by HUTCHINSON (1957). All maps were drawn at a scale of 1:2000. To construct a bathymetric map with a resolution of 5 m we follow the optimization criteria proposed by HAKANSON (1981) that required transects every 50 m. The drift of the boat was measured from shore at short intervals of time. An echosounder Japan Marina mod. 202 was used. The shore line contour was outlined from a centered aerial photograph, which was also used to draw a geomorphological map of the basin. The areas within depth contours were calculated by weighing scaled surfaces drawn in paper and the lengths within isopleths were obtained using the CTP (checkered transparent paper) method (HAKANSON, 1978). The lake volume was calculated by adding intervals between depth curves using a parabolic approximation, better suited for lakes with convex profiles. Area estimations had a reliability of 96% after applying the correction factors calculated as in HAKANSON (1981).

Data were gathered in 28 visits from May 30, 1984 to August 13, 1985. Sampling periods were selected to obtain similar variance in the studied factors between successive visits. Therefore, sampling was carried out every 15 days from the onset of

thermal stratification to the formation of the ice cover, every 20 to 30 days during the winter, when the intensity of change is reduced, and at weekly intervals from the time the thickness of the snow began to decrease up to the spring overturn. Meteorological data were collected from the Baserca Reservoir station (1500 m), that is close (4.5 Km), and within the same valley and similar orientation as the Redó basin. This station also has the longest data record of the nearby stations. The precipitation data of this station do not differ from those of other nearby stations (Lluset Reservoir, 2150 m; and Vaqueira, 1500 m) so that we expect it to reflect accurately the precipitation in the Redó basin. The precipitation data, however, may differ qualitatively from that in Lake Redó that should have a greater contribution of snow because of its greater altitude. Temperature differences in altitude were corrected by subtracting 1 for each 100 m of altitude difference.

There was no available data of incident radiation in the area near the lake. Consequently we used a theoretical approximation by modifying the Radiac program (GRACIA, 1983) to estimate the incident direct and diffuse radiation in the surface of the lake. Because the lake surface is flat, the model requires only the following input parameters: latitude; the atmospheric extinction coefficient; the horizon outline that is introduced as the vector of the angle formed by the subject with the crest line of the surrounding topography measured at 10 intervals; and the cloudiness, expressed in a scale of 10 of covered sky. Measurements of the atmospheric radiation extinction coefficient were obtained from the Jaca meteorological observatory (GRACIA, com. pers.) and cloudiness data from nearby Vaqueira meteorological station. Photosynthetically active radiation (PAR) was assumed to be 45-50% (KIRK, 1983) and ultraviolet radiation to be 6% (MILLER, 1981) of the total incident radiation.

Water transparency was measured with a 30 cm diameter Secchi disk. The light extinction coefficient (μ) can be approximated from transparency measurements using any of the existing relationships (see MARGALEF, 1983). Although the expression μD_s varies from 1.4 to 3.0, with a mean of 2.2 (REYNOLDS, 1984), we used the value of 1.7 (POOLE & ATKINS, 1929) because this appears to yield accurate results for high mountain lakes.

The quantity and quality of the light reaching the water surface in winter is influenced by the presence of ice and snow. There is no general relationship between the thickness of the ice and snow cover and the transmission of the light (ROULET & ADAMS, 1984). The proportion of light transmitted through the cover and the wavelengths most influenced depend on the nature of the different layers configuring the cover. Black ice has a low reflection index and is very transparent. Since it is usually not stratified internal refraction is limited to areas with air bubbles and other discontinuities. Recently deposited snow reflects from 70 to 90% of the incident radiation (RAGOTZKIE, 1978; ROULET & ADAMS, 1986), although reflection falls very rapidly upon deterioration (BOLSENGA, 1983). Because the ice and snow crystals of snow and white ice tend to have a somewhat random orientation they increase light scattering, resulting in increased light pathlengths and consequently greater light absorption. Despite this

TABLE 1. Light extinction coefficients (cm^{-1}) for different components of the winter cover of lakes (WILLIAMS, 1971; ADAMS, 1978; RAGOTZKIE, 1978; WEITZEL, 1983; REYNOLDS, 1984; ROULET & ADAMS, 1986). *Coefficientes de extinción de la luz en diferentes componentes de la cubierta invernal de los lagos (WILLIAMS, 1971; ADAMS, 1978; RAGOTZKIE, 1978; WEITZEL, 1983; REYNOLDS, 1984; ROULET & ADAMS, 1986).*

Water	0.0002	-	0.002	
Black ice	0.004	-	0.008	-0.015
White ice	0.06	-	0.07	
Snow	0.2	-	0.9	

complexity, the attenuation coefficients of ice and snow covers are restricted to a limited range (ALBRECHT 1964, after WETZEL, 1983; WILLIAMS, 1971; ADAMS, 1978; RAGOTZKIE, 1978; REYNOLDS, 1984; ROULET & ADAMS, 1986; table I).

We used these values in a conservative estimation of radiation transfer that considered the structure of the cover (CATALAN, in press) by using the smaller attenuation coefficients for each layer type. The extinction coefficient of slush must have an intermediate value between those of moderately turbid water (c. 0.002 cm^{-1}) and white ice (0.06 cm^{-1}), so we used these two values to obtain an interval comprising the true extinction coefficient. We did not consider in our calculations the reflexion that occurs in each interphase.

Vertical temperature profiles were obtained from the center of the lake in each visit to the lake by measuring temperature ($\pm 0.05 \text{ }^\circ\text{C}$) at 1 m intervals. Water density was calculated from the formulas provided by CHEN & MILLERO (1977) using a constant salinity of 0.00657‰ . The atmospheric pressure on the surface (P_s) was considered constant with a value of 0.7716 b obtained from the altitude of the lake (2240 m) (MORTIMER, 1981). The pressure at a depth z was considered $P_z = P_s + 0.09798 z$ (WETZEL, 1983), being P_z in bars and z in meters. According to this conditions, the temperature of maximum density on the surface of the lake is 3.97 and that of the bottom is $3.82 \text{ }^\circ\text{C}$.

CHARACTERISTICS OF THE BASIN AREA

The catchment of the lake has an amphitheatre-like shape and is surrounded by very steep rocky slopes, fitting the characteristics of a cirque. The drainage area (A_c) is 155 hm^2 , 90% of which is below 2500 m ASL (fig. 1). The average altitude of the watershed is 2397 m ASL, the Southern

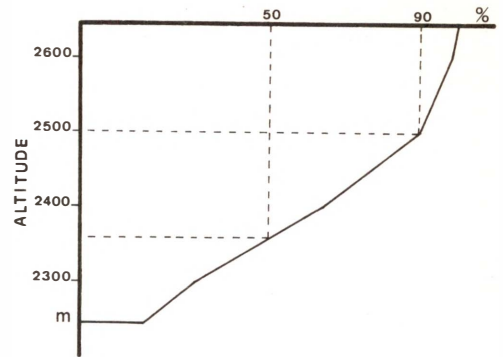


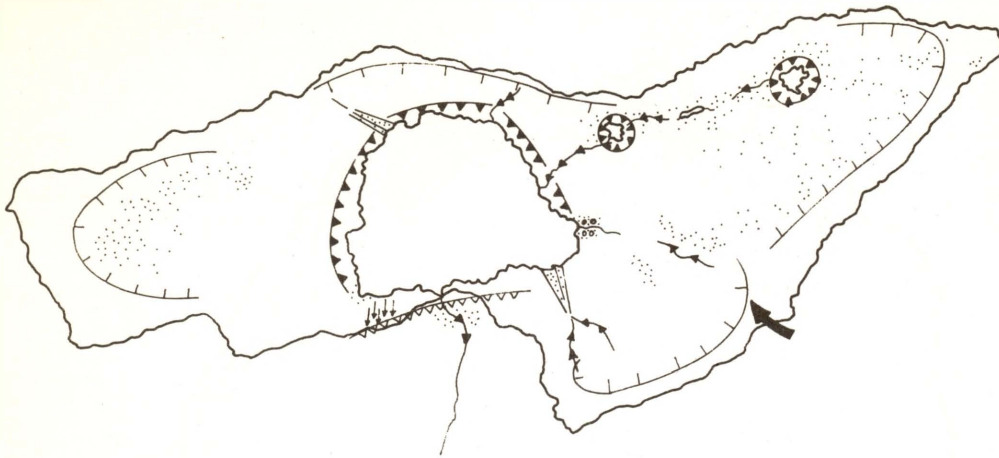
FIG. 1. Altitudinal distribution of Lake Redó drainage area. *Distribución en altitud del área de recepción nival del lago.*

portion being, on the average, 100 m lower than the Northern part.

The watershed is elongated in the East-West axis and the rock threshold, where the ice flow to the glacier occurred, is situated in the Southern portion (fig. 2). This configuration suggests that the ice advanced from the Sarraera and the Rius mountain pass in a West direction to join the ice masses coming from the Tuc del Port, that move East, in the center of the basin, where they continued a rotatory motion before flowing to the Southern rocky threshold. Such rotational movement could partially explain the considerable deepening of the basin close to the crest line.

The catchment relief is very rough with highly degraded shapes caused by intense periglacial dynamics; rock accumulations fill a large part of the basin. Two alluvial fans enter the lake through the Northwest and the Southeast respectively, locally altering the morphology of the lake basin (fig. 3). They remain active mainly because of the occurrence of avalanches.

The lake slopes steeply in the Northern and Western shores, and has a mixture of rock blocks and stones in the rest of the lake. There are some small beaches in the Southeast and the Southwest of the lake, together with the base of the Northwest alluvial fan, they are the only areas where fine, sandy materials accumulate.



- | | | | |
|---|--------------------------|---|---------------------------|
|  | Glacial cirque |  | Avalanche fan |
|  | Overdeepened basin |  | Screes |
|  | Glacial polished surface |  | Streams |
|  | Rock threshold |  | Fluviotorrential deposits |
|  | Glacial transflow pass |  | Lake, ponds |

FIG. 2. Geomorphological map of Lake Redó catchment. *Mapa geomorfológico de la cuenca del lago.*

The lake receives water from multiple sources, channelled through the fractures and accidents of the basin, without any of them dominating as a main inlet. Most inlets are only active during the thaw period and occasionally after intense rain in summer or autumn. The inlets that contribute water longer are: a Northeast inlet draining three small ponds in the foot of the Sarraera, that flows to the lake channelled through a large fracture; and another flowing to the lake through the Eastern beach, that drains the Rius mountain pass. Water inflow may fall below detectable levels in dry summers. The lake has a single outlet in the south part of

the basin that flows over the rocky threshold of the cirque.

The soils of most of the watershed are undeveloped because of the rock type (granodiorite), the cold climate, and the steep slopes. A substantial fraction of the surficial materials of the catchment is composed of bare rock or a lithosol overgrown by lichens or mosses. The rest of the catchment is covered by an incipient soil of the ranker (cryumbret) type: poor in clay, rich in humic acids, dark, that covers the bedrock which is only slightly decomposed.

The catchment of the lake has a vegetation characteristic of the acidophil

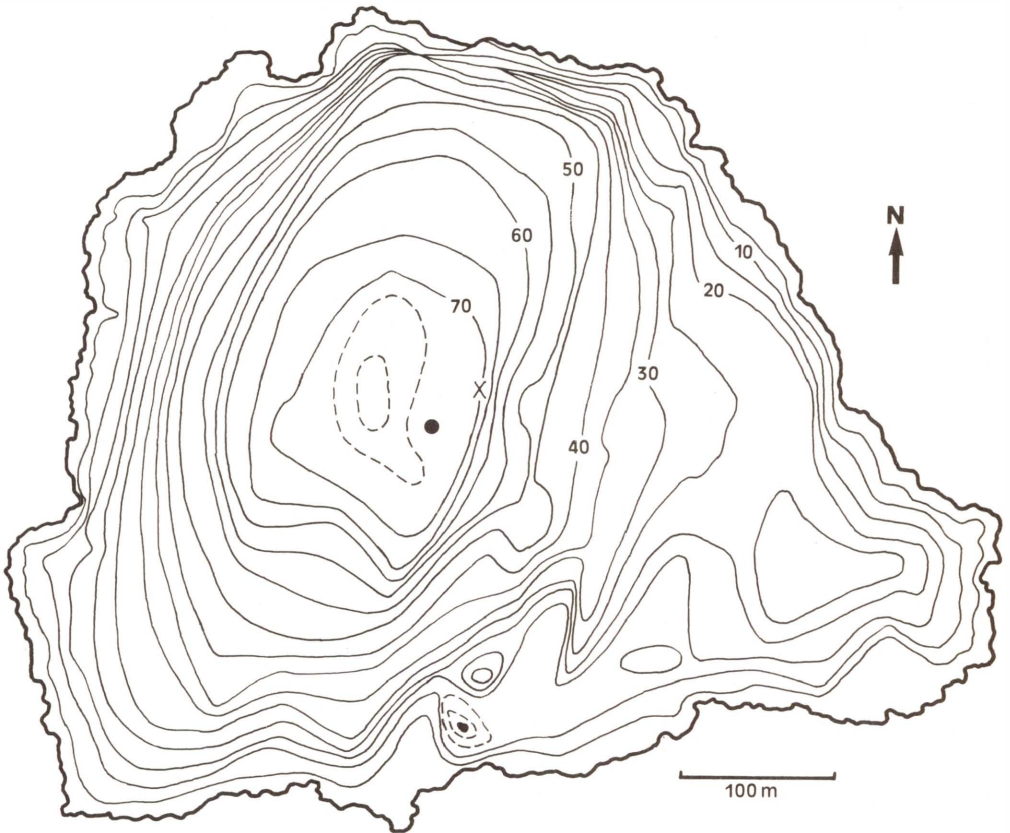


FIG. 3. Bathymetric map of Lake Redó, indicating the locations of the sampling station (X) and the maximum depth (O). *Mapa batimétrico del lago. Se indica el punto de muestreo (X) y el punto más profundo (O).*

TABLE II. Morphometric parameters. *Parámetros morfométricos.*

Lake Area (A)	24 hm ²
Maximum length (L _{max}) (NO-SE)	655 m
Maximum width (B _{max})	565 m
Shoreline length (L _o)	2.6 km
Maximum depth (z _{max})	73 m
Volume (V)	7.75 hm ³
Mean slope (I _m)	46 %
Catchment area (A _c)	155 hm ²
Mean width (B _m = A/L _{max})	369 m
Mean depth (z _m = V/A)	32 m
Relative depth (z _r)	13 %
(z _r = 100 x z _{max} / (2x(A/) ^{1/2})	
Shore development	1.5
(DL = 0.5 x L _o / (x A) ^{1/2})	
z _m /z _{max}	0.44
A _c /A	6.5
A _c /v	0.2 m ⁻¹

meadows (*Caricetalia curvulae*) of the alpine level of the Central Pyrenees (BALLESTEROS, in prep.). The formations of *Festuca eskia* and *Carex sempervirens* dominate the vegetation, although the microenvironmental diversity produced by differences in orientation and slope generates a mosaic of alternative communities.

The lake has been only slightly influenced by human activity. An outlet tube was located in the lake during the construction of the Vielha Tunnel in the middle of this century. The pipe has a diameter of 45 cm and draws water from a depth of 4 m, but it makes a siphon at about 0.5 m of the maximum lake level.

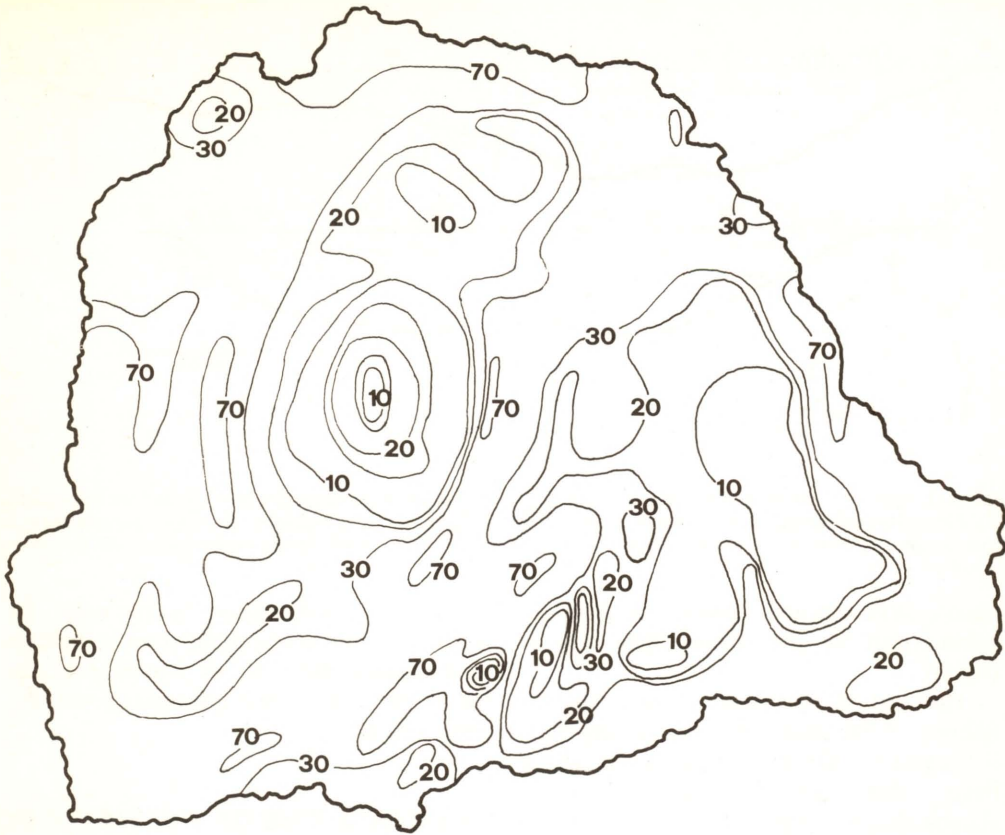


FIG. 4. Slope (%) distribution of the bottom of Lake Redó. *Mapa de pendiente del lago (%)*.

Originally, the flow through the tube could be regulated, although the mechanism is now out of service and the floodgate remains permanently half open. The outflow from the tube is only interrupted when the lake freezes out in winter or in very dry summers when the level of the water falls below the level of the siphon.

MORPHOLOGY OF THE LAKE

The bathymetric map (fig. 3) and the morphometric parameters of the table II reflect the morphological characteristics of the lake basin. This lake (24 hm^2) is large relative to other Pyrenees lakes (MARGALEF *et al.*, 1975), although in a more general context it has to be considered small. Its sub-circular shape, typical of

cirque lakes, is reflected in the value of the shore development (table II) that approaches very closely that for cirque lakes (HUTCHINSON, 1957). The greater asymmetry is to the Southeast of the lake, where there is a sub-basin and where the slope is less steep than in the rest of the lake (fig. 4).

The lake is remarkably deep in relation to its area, resembling other lakes that experienced exceptional over-deepening, such as some lakes of the Lofoten range in the Moskenesoy islands (HUTCHINSON, 1957). There is a small promontory in the middle of the main basin that reaches 8 m above the level of the bed (fig. 3, 5). Its whaleback shape resembles the *roche moutonnés* formations typical of glacial landforms, and it may be a result of a change in the glacier direction. The

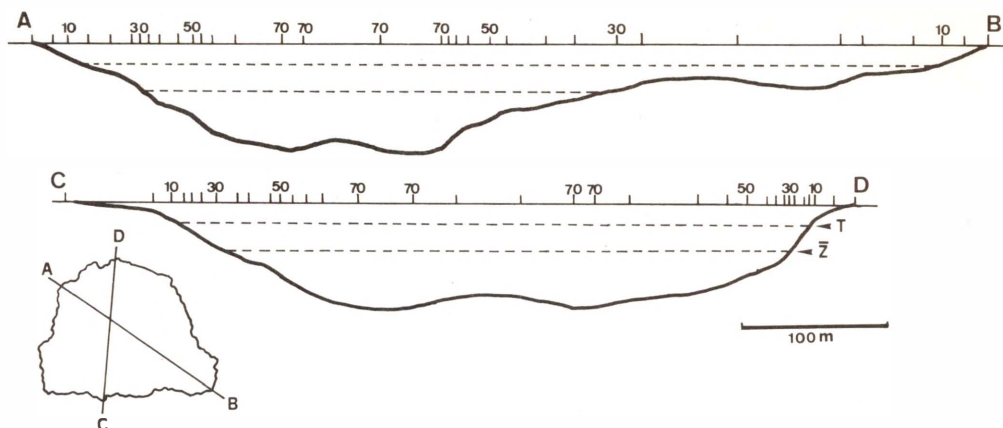


FIG. 5. Longitudinal sections of the lake showing the position of the summer thermocline (T) and the mean depth (Z). Horizontal and vertical axes are drawn at the same scale. *Secciones longitudinales del lago que ilustran la posición de la termoclina en verano (T) y la profundidad media (Z). La escala del eje horizontal y la del vertical es la misma.*

variations of area and volume with depth are summarized by the hypsographic curves (fig. 6).

The bed of the basin is only slightly uneven on the whole. Its greater roughness is caused by the large rock blocks which have fallen into the lake and the accumulation of large boulders (8-140 cm).

The very steep relief of the basin determines the occurrence of important episodes of coarse sediment input during thaw and torrential rains. The extent of wave action and currents is small and decreases rapidly with depth in lakes of these dimensions (SLY, 1978). Consequently, the energy levels permit only a limited transport of the sedimentary materials that enter the lake. The critical depth below which sediment accumulation should predominate must lie about 1 m, considering that wind action is limited to an effective fetch shorter than one kilometer (HAKANSON, 1982a). In this lake, the deposition processes are determined by the bottom slope, with the exception of a very narrow littoral strip. The slope profile (fig. 7) clearly shows that the lake is a very efficient sediment trap. Because fine material only accumulates on slopes < 4.6% (HAKANSON, 1981) they must be highly localized at considerable depths in the lake

(fig. 4, 7). Obviously, there must be localized sediment accumulation in bottom irregularities, although we cannot evaluate the importance of these phenomena with the data in hand.

RESIDENCE TIME OF THE WATER IN THE LAKE

FIRST APPROXIMATION

In relatively small lakes, the water residence time provides an indication of the relative importance of advective processes in the distribution of water mass properties (CARMACK *et al.*, 1986). The precise determination of lake water residence times is complex and involves the precise estimation of their hydrological behavior, including high quality data on precipitation, input and output flows, air temperature and humidity (CHOW, 1964). However, a first approximation can be made on the basis of the annual precipitation, by assuming water residence time (T_r) to equal the ratio V/S , where V is the volume of the lake and S is the outflow rate of water. Assuming all precipitation falling in the basin to reach the lake, water residence time would range from 4.2 years in years of normal precipitation (c.

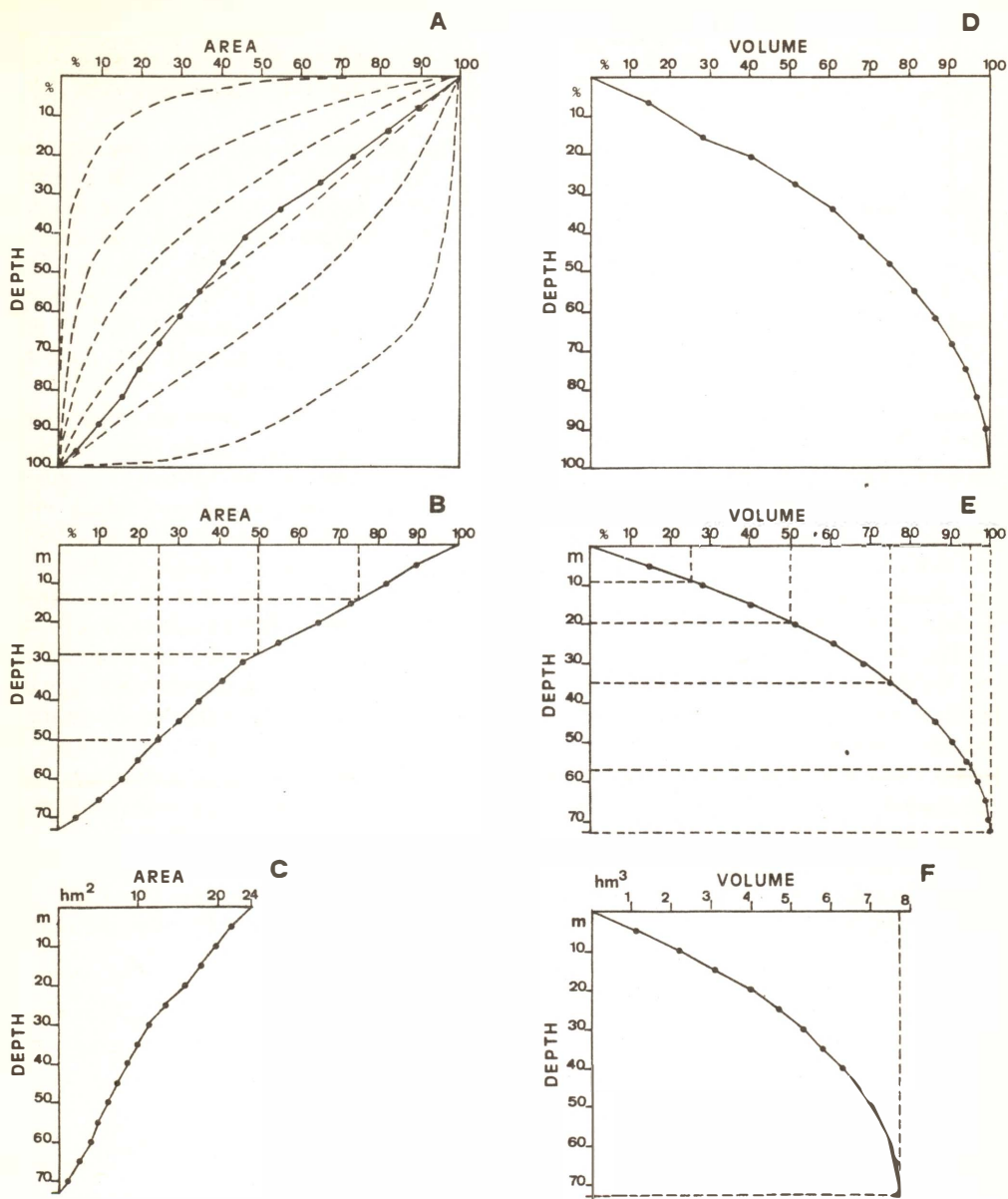


FIG. 6. The areal (a,b,c) and volumetric (d,e,f) hypsographic curves of Lake Redó. *Curvas hipsográficas de área (a,b,c) y volumen (d,e,f) del lago.*

1200 mm) to 3 years in the years with exceptionally high precipitation (c. 1700 mm). With this long water residence time wind action and heat exchange must be the main factors influencing the vertical structure of the water column, as has been stated in other works (MORTIMER, 1984).

ASPECTS OF THE HYDROLOGICAL CYCLE IN A SPECIFIC PERIOD (8/8/84-8/8/85)

There are two important events in the hydrological cycle of the lake: the autumn storms and the spring thaw. During the

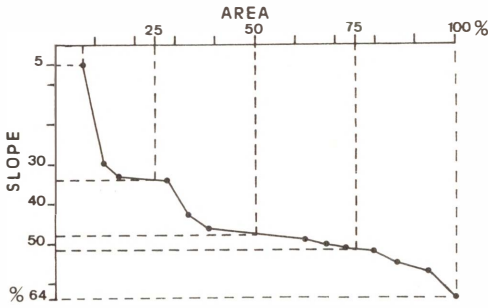


FIG. 7. The areal distribution of bottom slopes (%) in Lake Redó. *Porcentaje de área en referencia a la pendiente (%)*.

autumn storms recorded along the studied period the lake level increased several centimeters in two occasions (October 2, and November 19). A substantial fraction of the annual precipitation (25%) occurred during the first fortnight of November (fig. 8). This event must have influenced severely the residence time of the water column, because the mixed layer reached down to the lake bottom in that period. The steep slopes of the catchment, the poorly developed soil, and the low permeability of the granodiorite, together with the torrential nature of the rain, caused a large fraction of the precipitation to reach rapidly the lake. Further, the wide distribution of the water

input throughout the lake facilitates the mixture of the inflowing water with lake water.

The increase of the water level during thaw differed substantially from the autumn increases. About 30 to 40% of the annual rainfall fell from the time the lake froze (mid December) until outflow resumed (end of May), and a further 5 to 10% fell during thaw. Consequently, about 50% of the annual precipitation entered the lake in approximately one month.

The lack of information on infiltration, evaporation and sublimation rates in the catchment makes it very difficult to evaluate the fraction of the precipitation falling into the basin reaching the lake. WOO (1985) has estimated the evaporation plus the evapotranspiration to be 40% of the rainfall in Canada, and SCHINDLER *et al.* (1974) estimated it to be 15% for an Arctic lake. Because of the steep slopes and rock type of the Redó basin I estimate that the fraction of the annual precipitation reaching the lake is probably no more than 80% of the total.

Snow melt started earlier in the basin than in the lake, due to the effect of the lower ice. The resulting water flowed to the lake raising its level. Then the lake cover split on the edges (fig. 9), specially near the outlet

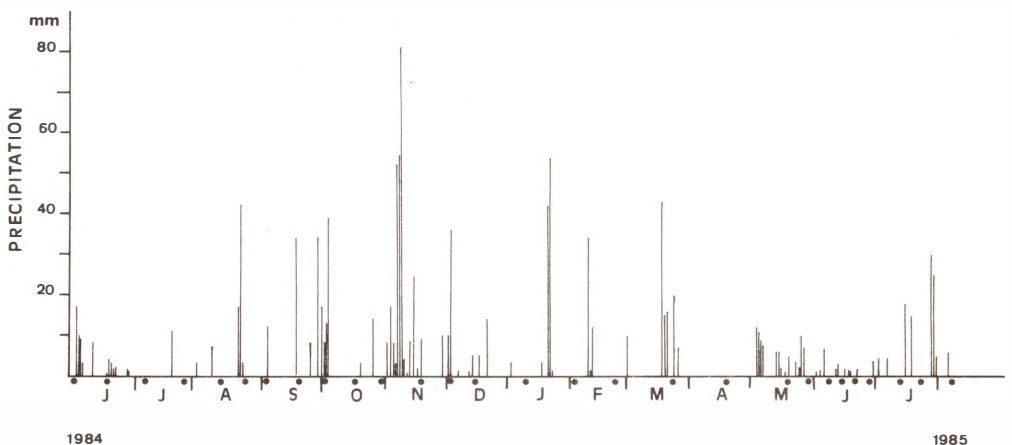
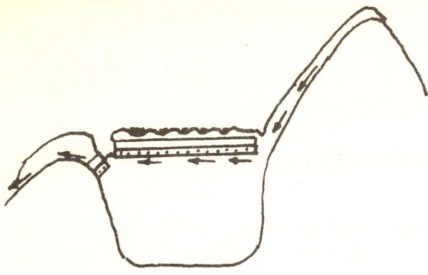
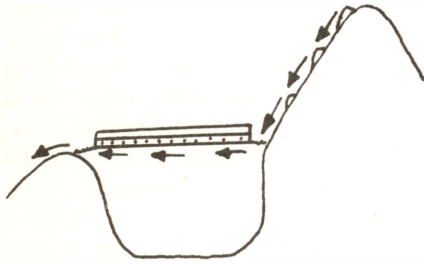
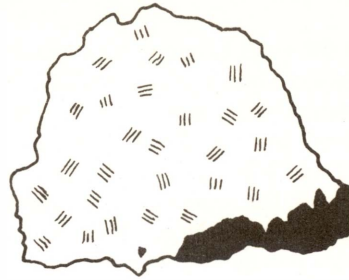


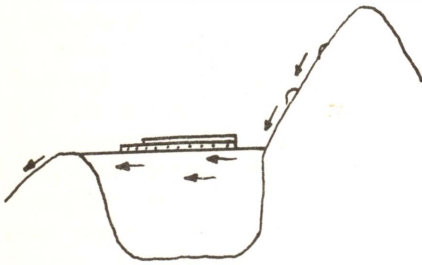
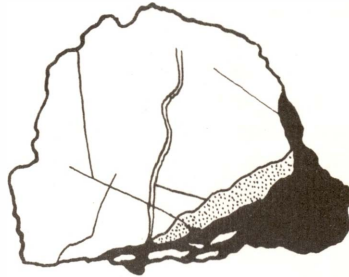
FIG. 8. Temporal sequence of atmospheric precipitation recorded at the Baserca meteorological station (ENHER) during the studied period. This meteorological station is located in the same valley as Lake Redó, at a distance of 4.5 km. Dots indicate sampling days. *Precipitación en la estación meteorológica de Baserca (ENHER) durante el período estudiado. Esta estación está situada a 4.5 km del lago, en el mismo valle. Los puntos indican días de muestreo.*



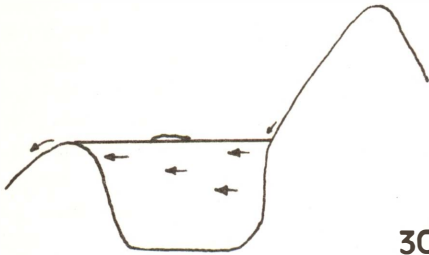
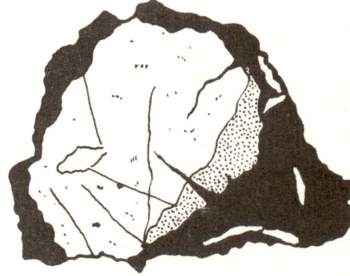
1rst



7th



15 th



30 th



FIG. 9. Diagrammatic representation of the melting process of the winter cover during June 1985. Left, longitudinal section of the basin showing water circulation. Right, areal view of the lake showing thawing and breaking-up of the cover. Further details are provided in the text. *Esquema del proceso de deshielo en Junio de 1985. Izquierda, sección longitudinal de la cuenca mostrando la circulación del agua. Derecha, visión superficial del lago mostrando el deshielo y la ruptura de la cubierta. En el texto se describe el proceso con detalle.*

where the water began to flow. This process accelerated rapidly, and water level reached the annual maximum (0.5 m above the minimum level at the end of the summer recorded in 1984, 1985, 1986) in a week. A week later the water level dropped a few decimeters and a large sheet of black and white ice remained occupying three quarters of the lake surface. Thus, the variation in water level and outflow during the first weeks of thaw is a result of water melting in the basin rather than of ice melting in the lake. In the thaw of 1985 (towards June 20) the ice cover that had been drifting in two or three large blocks for a few days, fragmented further to cover the lake with elongated floes (c. 10 m) characteristic of thaws from covers with a lot of snow and white ice (WOO, 1985). As a result of wind action the floes oscillated from side to side of the lake. This situation occurred in early July of 1984, probably because the thickness of the snow and ice cover was twice that of the following year. The thaw period ended a week after this situation, although snow banks scattered throughout the perimetry of the lake melted throughout July. Water produced during thaw approached the lake flowing between the rocky substrate and the snow thereby remaining at temperatures below 1° C. The water entered the lake flowing under the ice cover. Because the snow of the basin melted faster than the ice cover, a strong vertical temperature gradient remained while the melted water entered the lake. In the second half of the melting period, more thaw water flowed to the lake over rocky surfaces, increasing its temperature (2-3 °C) in the process, such that it penetrated to a greater depth. At this point vertical mixing was enhanced by a reduction in the vertical density gradient and by the influence of convection generated by the interaction of direct solar surface water heating and simultaneous cooling due to the influence of ice blocks advected by the wind. The great thermal variability characteristic of this situation is exemplified by temperature fluctuations from 3-4 °C to

< 1 °C at a fixed station following the passage of an ice floe.

STRATIFIED WATER RESIDENCE TIME

Increased accuracy in the calculation of water residence time may be achieved by considering the vertical structure of the water column. In order to calculate water residence times the lake can be divided in different layers (MARGALEF, 1983). Because water input and output are surficial phenomena the upper water layers turn over faster than deeper layers. This differential behavior is enhanced as water exchange between different layers decreases. To allow the stratified calculation of water residence time we adopted the following assumptions: (1) the precipitation in the basin was assumed to be 30 % greater than that recorded at the Baserca meteorological station to allow for situations of greater precipitation; (2) evapotranspiration plus evaporation rates were taken to be constant at 15% of the annual precipitation; (3) underground exchanges of water were assumed to be negligible; (4) water outflow was assumed to occur only at the outflow and outflow tube. Surficial water outflow was estimated from the river cross-section and current speed (c. 0.1 m/s) measurements performed in each visit, whereas outflow through the tube was assumed to be constant throughout the year, excepting those periods when no flow was observed. We calculated the outflow through the tube to be 8166 m³/d by distributing the annual precipitation in the basin over the 197 days where inflow to the lake was observed, and accounting for evapotranspiration and evaporation losses and surficial outflow. Obviously this calculations would tend to overestimate flow at low lake stages and underestimate it at high lake stages; (5) we assumed that water inflow and outflow during vertical stratification influences only the residence time of epilimnetic layer. The thickness of the water column influence by inflow-outflow processes during thaw was

TABLE III. Calculation sheet of the stratified mean residence time of the lake. *Estima del tiempo de residencia medio de diferentes capas de agua del lago.*

Layer (m)	TR (years)
0-5	1.9
5-10	2.4
10-15	3.4
15-20	5.3
20-40	9.7
40-73	15.5

assumed to be over 10 m the first week, 20 m the second week, and all entire water column in the following ones. The results of these calculations are reflected on table III. The water residence time obtained is subject to considerable uncertainty, although consideration of alternative hypotheses do not lead to substantially different results.

RADIATION

EFFECT OF THE MOUNTAINS ON THE DISTRIBUTION OF RADIATION

The central area of the lake is the least influenced by surrounding mountains, and therefore is the area that approaches more closely an ideal flat surface. Assuming a cloudless sky and no influence by surrounding mountains, Lake Redó would receive, on the average, an annual irradiance of 269 W m^{-2} . Shading by surrounding mountains would reduce this figure down to 257 W m^{-2} . Because of the profile of the mountains surrounding Lake Redó shading at the center of the lake is greater in September (Fig. 10). The relative distribution of the radiation on the lake surface varies seasonally (fig. 11) due to variations in the effect of shading by mountains caused by changes in the trajectory of the Sun. The Southeast shore of the lake, where the beginning of thaw occurs (fig. 9), receives more radiation from March to October, whereas it is the portion of the lake that receives the least radiation when solar angle is low (November to February).

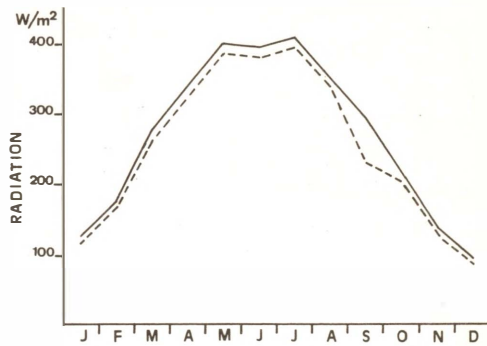


FIG. 10. The influence of mountain shading upon the maximum potential incident radiation received at the centre of the lake. The solid line represents the radiation calculated ignoring mountain shading, and the broken line represents the radiation calculated after correcting for mountain shading. *Efecto de las montañas sobre la radiación incidente potencialmente máxima en el centro del lago. Radiación sin montañas, línea continua; radiación con montañas, línea discontinua.*

INCIDENT RADIATION

The maximum potential radiation is modified by cloud cover. Cloudiness data for the period when field work was carried out (January 1984-August 1985) shows that intermediate cloudiness was infrequent (fig. 12). In general, summer months have a lower average cloudiness, although clear skies are also possible for other months (i.e., October 1984 or February 1985). After accounting for cloud cover, the average annual radiation in the center of the lake was 66% (i.e. 169 W m^{-2}) of the maximum potential value. The maximum average monthly irradiance occurred in July (300-330 W m^{-2}) and the minimum in November (40-80 W m^{-2}) (fig. 13).

The proportion of diffused radiation varies throughout the year, increasing when the radiation has to cross through a thicker atmospheric layer. The diffusion of light also increases with cloudiness: a half-covered sky raises the diffuse fraction to a 30-40% of the total. Logically, the net effect of cloudiness is more important during the periods of the year with greater radiation.

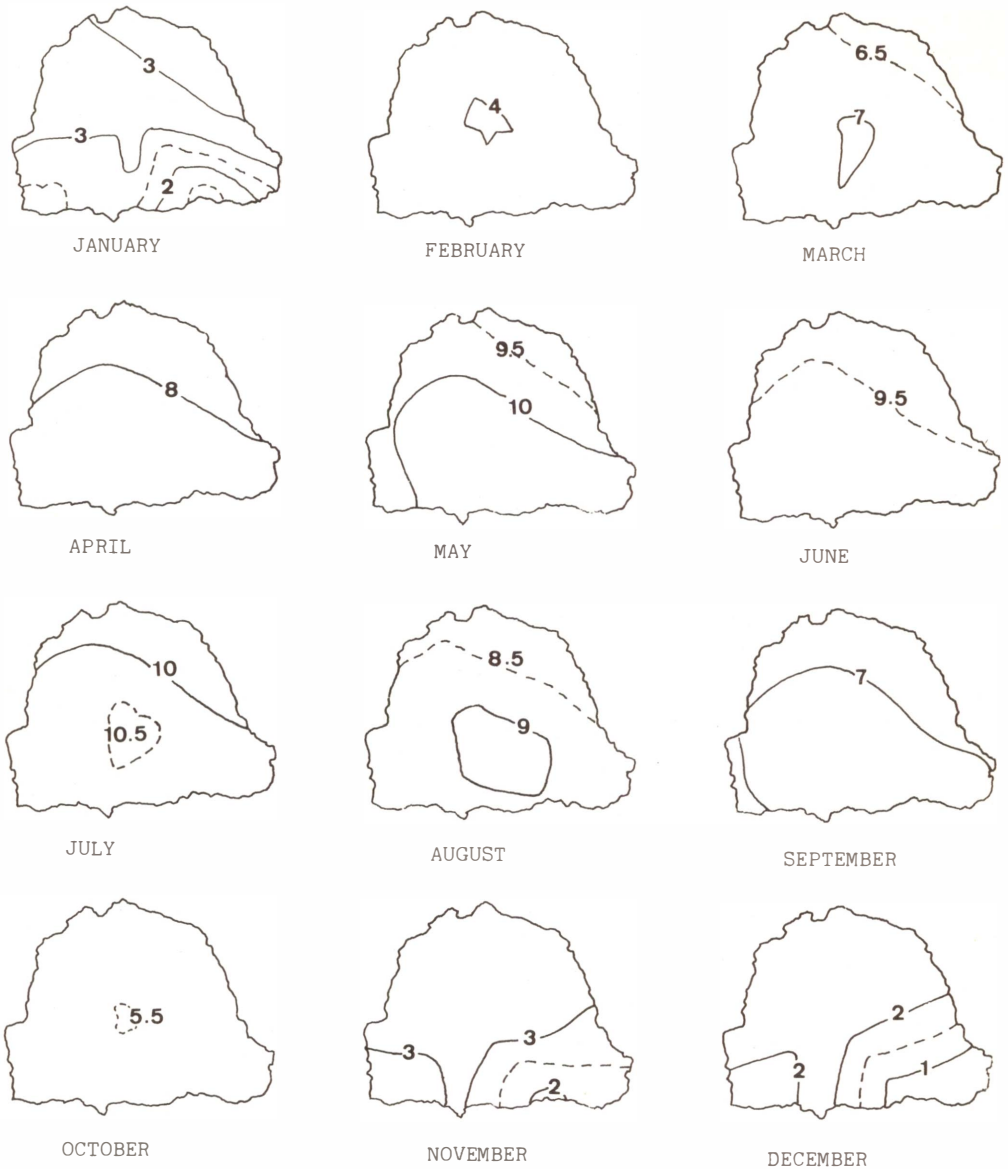


FIG. 11. Seasonal and spatial variation of the maximum potential radiation received at the lake surface ($10^8 \text{ J m}^{-2} \text{ month}^{-1}$). *Variación estacional y espacial de la radiación incidente potencialmente máxima en la superficie del lago ($10^8 \text{ J m}^{-2} \text{ mes}^{-1}$).*

When conditions are optimal (i.e., ice-free water surface, clear skies) the incident radiation during the hours of peak intensity approaches 1200 W m^{-2} (a value of 1185 W m^{-2} has been recorded at a similar latitude (GÉNOVA, *com. pers.*), that approaches the solar constant (1390 W m^{-2}).

UNDERWATER LIGHT ENVIRONMENT

The fraction of the incoming radiation reaching the water surface reflected to the atmosphere depends on the incidence angle. Light reflection ranges from 2-3% for angles between 0° and 50° , but light reflection

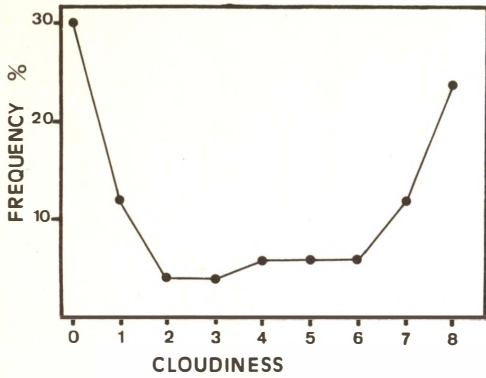


FIG. 12. Frequency distribution of cloudiness (1/8 of covered sky) recorded in the Vaqueira meteorological station for the studied period. *Distribución de las frecuencias de nubosidades (octavos de cielo cubierto) durante el período de estudio; datos de la estación meteorológica de Vaqueira.*

increases rapidly as greater angles are reached (e.g., 70°, 13%; 80°, 35%; 89°, 90%). Further, the light reflection at high incidence angles decreases as a function of wind speed (KIRK, 1983). The average proportion of radiation reflected for Lake Redó is about 3%, because shading by surrounding mountains obliterates all direct radiation at sun angles equal or greater than 80.

Maximum underwater light penetration (1% of the light reaches 50 m) was recorded during August and September, and

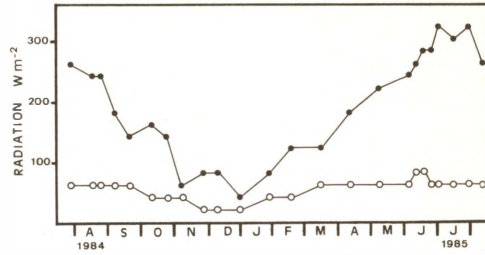


FIG. 13. The temporal sequence of the estimated mean incident radiation received between sampling intervals. *Radiación incidente media estimada para intervalos entre muestreos.*

decreased in Spring and Autumn (fig. 14), although the reasons for the decrease differed for these two periods. The depth of disappearance of the Secchi disk is often related to the average chlorophyll concentration above that disk (fig. 15a). A linear function fitted our data closely ($r^2=0.71$) than a power function ($r^2=0.61$) typically used to describe this relationship (MARGALEF, 1983). Closer examination of our data permits their differentiation in two groups: (1) a group comprising the observations recorded from mid August to lake freeze up, when water transparency is strongly related to the chlorophyll concentration (fig. 15b), and (2) a period comprising the thaw and the stratification onset when water transparency is not

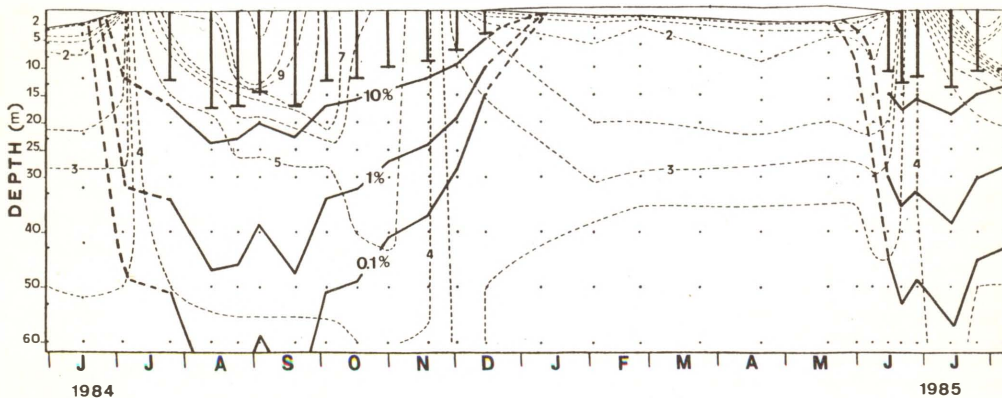


FIG. 14. Seasonal variation of the transparency and temperature in Redó lake. *Variación estacional de la transparencia del agua y de la temperatura en el lago.*

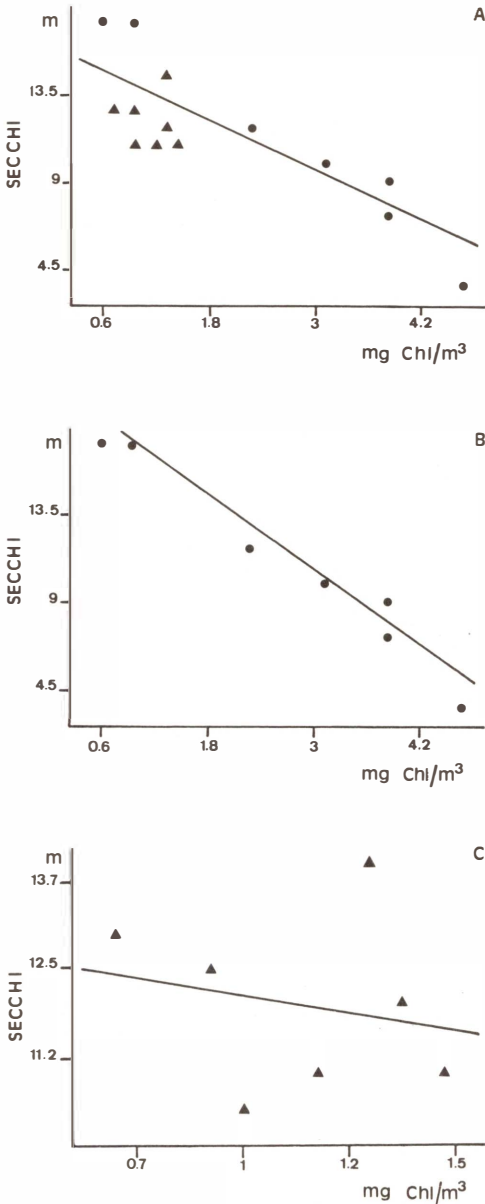


FIG. 15. Relationship between the depth of Secchi disk transparency and the average chlorophyll concentration above this depth. (A) The relationship for the ice-free period ($r^2 = 0.71$, sig. 0.0002). (B) The relationship for sampling dates far from thaw ($r^2 = 0.97$, sig. 0.0001). (C) The relationship for sampling dates near thaw ($r^2 = 0.04$, sig. 0.66). *Relación de la profundidad de desaparición del disco de Secchi y la concentración media de clorofila por encima de esa profundidad. A) Datos para todo el período libre de hielo ($r^2 = 0.71$, sig. 0.0002) B) Datos para días de muestreo alejados del deshielo ($r^2 = 0.97$, sig. 0.0001). C) Datos para los días de muestreo cercanos al deshielo ($r^2 = 0.04$, sig. 0.66).*

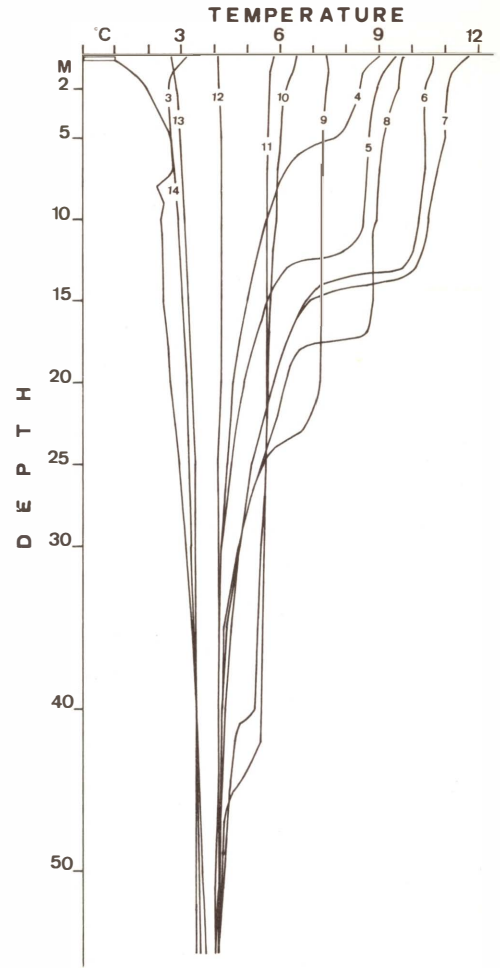


FIG. 16. Vertical temperature profiles showing the formation (3-7) and decay (7-14) of thermal stratification during the ice-free period of 1984. *Perfiles verticales de temperatura que ilustra la formación (3-7) y la destrucción (7-14) de la estratificación térmica durante el período libre de hielo de 1984.*

significantly related to the chlorophyll concentration (fig. 15c). Water transparency decrease in the latter period is attributable to enhanced light scattering due to thaw water and the loading of suspended inorganic materials.

When the lake surface froze up, the resulting black ice absorbed very little radiation (table IV), although the uneven distribution of the first snow on its surface resulted in a heterogeneous light environment. However, rapid snow

accumulation reduced the penetration of light enough to presumably prevent photosynthesis. This situation persisted until early June when the cover cracked, producing a sudden increase in underwater radiation. Horizontal heterogeneity in underwater radiation increased during the thaw process due to the contrast between the high irradiance penetrating the portions of the lake devoid of ice cover and the much lower, although probably sufficient to support photosynthesis, irradiance under the melting cover.

CHARACTERISTICS OF THE ANNUAL THERMAL CYCLE

The thermal cycle of Lake Redó characterize it as a dimictic lake (fig. 14). Solar heating and wind induced mixing increased stratification from spring overturn until August, when the maximum surface temperature was reached (12 °C in 1984 and 15 °C in 1985).

The epilimnion, with water temperatures comprised between 8 and 12 °C, extended down to 11 m, the summer thermocline reached down to 13 m, and delimited the hypolimnion with temperatures between 7 and 4 °C. Water temperatures below 25 m remained < 6 °C throughout the year.

The decrease of incident radiation registered in September resulted in considerable heat loss on the upper layers, increasing the thickness of the epilimnion by eroding and weakening the thermocline (fig. 16).

By the end of October the mixed layer reached down to 40 m. Fall overturn initiated by mid November and persisted to the end of the month, when an inverse temperature stratification set up (fig. 14). The lowest hypolimnetic temperature (3.4 °C) was reached during the mixed period, and bottom temperatures increased slightly following inverse stratification due to sediment heat loss. The month previous to freezing was characterized by an important

TABLE IV. Calculations of light penetration through the winter cover. *Estima de la transmisión de luz a través de la cubierta invernal.*

Date	Transmittance %
15/12/84	50 - 95
19/04/85	4.7 x 10 ⁻⁶ - 0.03
15/12/84	50 - 95
12/01/85	0.2
3/02/85	1.7 - 3 x 10 ⁻⁶
23/02/85	0.002 - 0.04
23/03/85	8 x 10 ⁻⁵ - 0.01
19/04/85	4.7 x 10 ⁻⁶ - 0.3
19/05/85	5.3 x 10 ⁻⁶ - 0.03
1/06/85	0.07 - 0.2
8/06/85	2.5
15/06/85	39

negative heat flow (c. -100 W m⁻²), coinciding with the minimum incident radiation. The lake froze by mid December. The lowest heat content of the lake occurred - considering the ice and snowcovers to be external to the lake - in the second week of April, although there was an ephemeral minimum during thaw (fig. 17). RAGOTZKIE (1978) postulated the occurrence of this minimum during thaw, and attributed the paucity of knowledge on this phenomenon to the difficulties involved in sampling at that time.

Once most of the snow from the lake and its basin melted down the remaining ice could not compensate the heating caused by the incident radiation and the lake rapidly gained heat and became stratified, such that the spring mixing period was shorter than the fall one.

The annual thermal budget (sensu Birge, 1915) was calculated to be 15211 cal cm⁻² y⁻¹ (20.21 W m⁻²) for 1984. This budget can be decomposed in a fraction of 9990 cal cm⁻² necessary to bring the lake from spring isotherm up to its maximum heat content, and 5221 cal cm⁻² necessary for the heat change from the minimum heat content up to spring isothermy. The heat stored in the water column during isothermy was about 12800 cal cm⁻².

The latent heat in the ice and snow cover during the winter maximum was estimated to be 4781 cal cm⁻² for the winter 1984-85 (CATALÁN, *in press*).

ESTRUCTURE OF THE WATER COLUMN

From a mechanical perspective, the thermal structure of the lake must be considered as density gradients and, particularly, as the resistance of a water layer to an angular or lineal disturbance. The frequency of Brt-Vs(N) is a good indicator of the mechanical resistance of a layer to mixing.

$$N^2 = (g \, d\sigma/dz) / \sigma_0$$

Where g is the acceleration of gravity, σ_0 is the mean density and $d\sigma/dz$ is the density gradient. The values of this index differentiated several periods in the vertical structure of the water column of Lake Redó (fig. 18). An important summer peak of N^2 slitted the column, with diverse stability

situations above it. The values of N^2 decreased during fall and the N^2 maximum became progressively deeper until vertical stratification was totally lost. The N^2 gradient was located immediately under the ice in winter. Finally, the instability of the column during the thaw period was reflected in negative N^2 values, particularly in the upper layers (profile of 6 July, 1984), indicating that the lake was displaced from its vertical equilibrium.

AGENTS GOVERNING THE EXCHANGE OF ENERGY DURING THE PERIOD WITHOUT ICE COVER

WIND

Wind action is an important factor for the transference of energy from the atmosphere

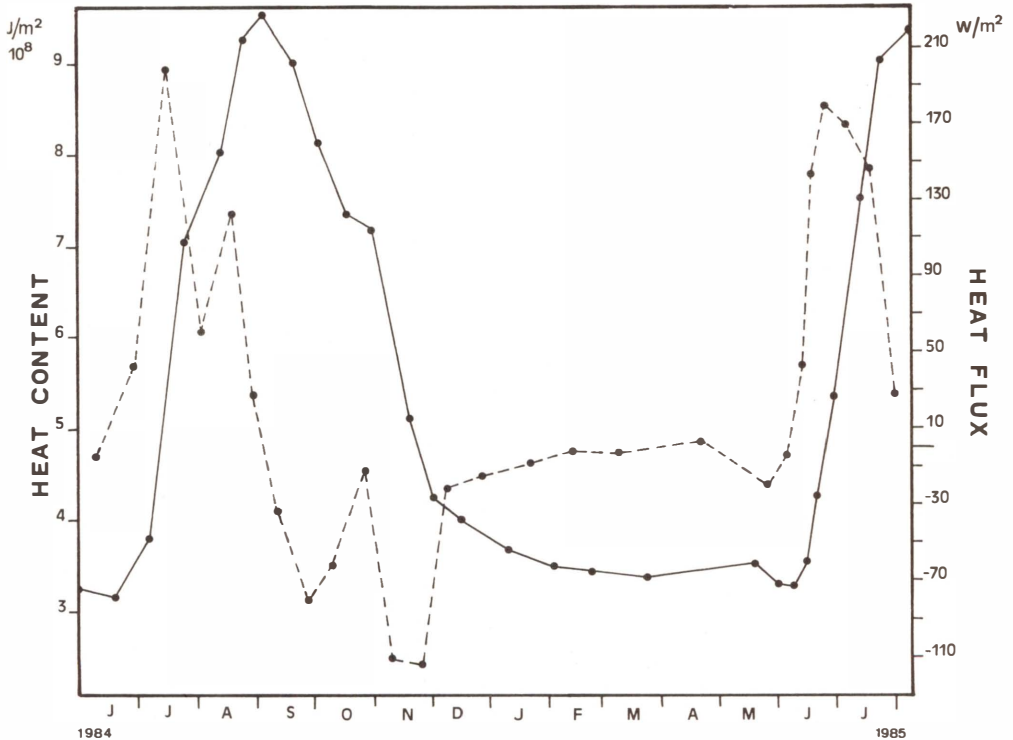


FIG. 17. Temporal sequence of lake heat content (solid line) and heat flux (broken line) for the studied period. *Contenido de calor del lago (línea continua) y flujo de calor (línea discontinua) durante el período estudiado.*

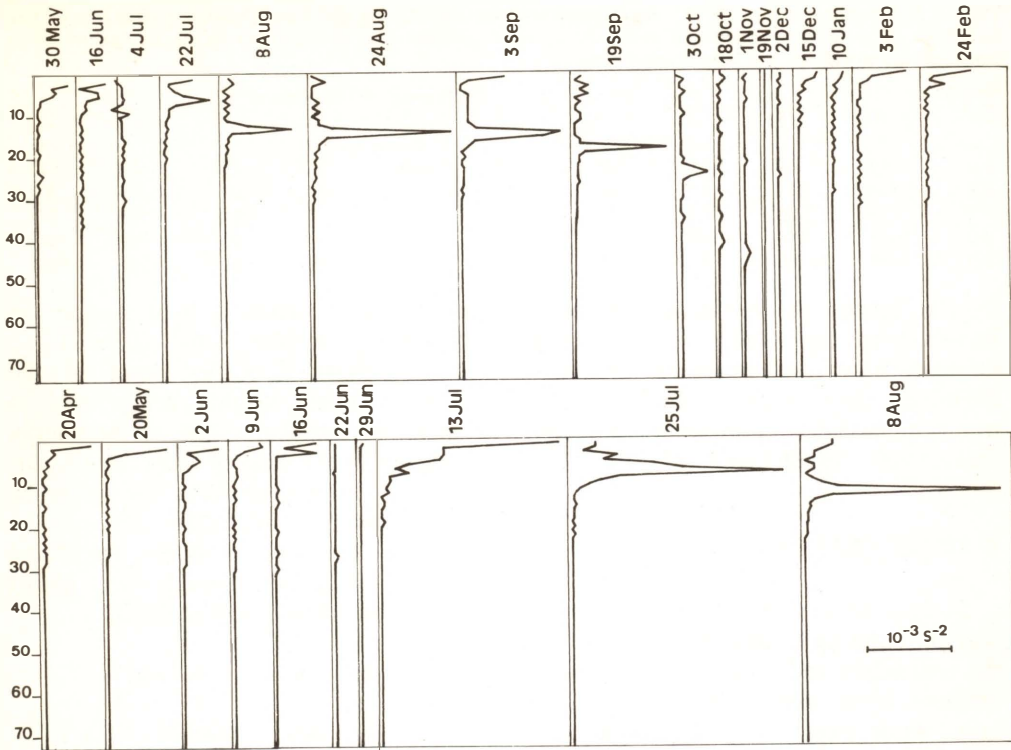


FIG. 18. Vertical profiles of the square Brunt-Väisälä frequency. *Perfiles verticales del cuadrado de la frecuencia de Brunt-Väisälä.*

to the water, both because of its mechanical action and because of its influence upon the processes of evaporation and exchange of sensible heat. The mechanical effect of the wind can be characterized by the turbulent friction velocity,

$$U^* = (\sigma_a C_d v^2 \sigma_s^{-1})^{1/2}$$

where σ_s , σ_a are the densities of surface water and air (0.96 kg m^{-3}), v is the wind speed at a reference height above the water surface and C_d is the drag coefficient (1.3×10^{-3} , for small lakes: FISHER *et al.*, 1979).

The wind speeds most frequent in the area are around 3.5 m s^{-1} , with wind speeds in the order of $1.5\text{-}7 \text{ m s}^{-1}$ (fig. 19) being common while wind speeds $> 10 \text{ m s}^{-1}$ are far more sporadic. For a given wind speed, the density of the lake surface only changes

U^* in 10^{-6} ms^{-1} . Consequently, wind speed is the main determinant of the velocity of turbulent mixing by friction. The values of U^* span over an order of magnitude. Because of the subcircular shape of Lake Redó wind direction is relatively unimportant. South or Southeast winds, however, have a differential influence across

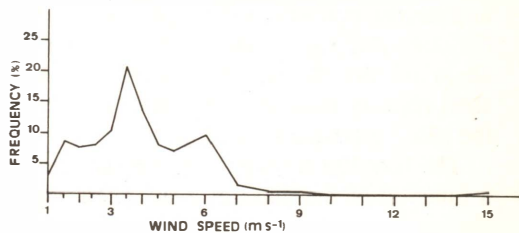


FIG. 19. Wind speed distribution in the Southern Mouth of the Tunnel of Vielha (MOPU) for the ice-free period of 1984. *Distribución de las velocidades del viento en la Boca Sur del Túnel de Vielha (MOPU) durante el periodo libre de hielo de 1984.*

TABLE V. Sensible heat flux ($W m^{-2}$) for different combinations of wind speed and air-water surface temperature difference. *Flujo de calor sensible ($W m^{-2}$) para distintas combinaciones de velocidad del viento y diferencia de temperatura entre el aire y la superficie del agua.*

cWind m s ⁻¹	Difference of Temperature °C									
	-20	-15	-10	-5	-2	2	5	10	15	20
1.0	113	84	56	28	11	-11	-28	-56	-84	-113
3.5	394	295	197	98	39	-39	-98	-197	-295	-394
6.0	675	506	338	169	68	-68	-169	-338	-506	-675
9.0	1013	760	506	253	101	-101	-253	-506	-760	-1013
15.0	1688	1266	844	422	169	-169	-422	-844	-1266	-1688

the lake because the lake is not isotropically sheltered by the relief. This differential influence must result in uneven sinking of the mixing layer throughout the lake leading to compensatory horizontal advective movements (IMBERGER & PARKER, 1985).

SURFACE HEAT EXCHANGE

Surface heat exchange can be divided into different processes. Evaporation, and the conduction and exchange of long-wave radiation occur only at the most superficial layer, while shorter wave lengths penetrate the water column according to the bulk irradiance extinction coefficient.

The sensible heat transfer resulting from temperature differences between air and water can be evaluated through the aerodynamic formula (GILL, 1982),

$$Q_s = -\sigma_a c_p Ch v (t_s - t_a)$$

where c_p is the specific heat ($4.194 J kg^{-1} \text{ } ^\circ C^{-1}$), Ch is the drag coefficient (1.4×10^{-3} , IMBERGER & PATTERSON, 1981), and t_s and t_a are the temperature of surface water and air, respectively. The range of values for Q_s for different wind and temperature situations are illustrated in Table V. We shall refer to positive heat fluxes whenever the lake experiences a heat gain.

The heat lost through evaporation (Q_e) is a function of the mass of evaporated water (Ev),

$$Q_e = -(L_h Ev + c_p \sigma_s Ev (t_s - t_a))$$

where L_h is the latent heat of evaporation ($L_h (J kg^{-1}) = 2.50086 \times 10^6 - 2.3 \times 10^3 t_s$, (GILL, 1982)). The first term of the expression refers to the energy used in evaporation and the second to the energy transferred by the mass of evaporated water. The second term achieves values much smaller than the first term, and can be neglected. The mass of water evaporated can be calculated through the global aerodynamic formula (GILL, 1982):

$$Ev = \sigma_a C_e v (q_s - q_a)$$

where C_e is a drag coefficient (1.5×10^{-3}). The specific humidity at surface level (q_s) is assumed to equal the saturation humidity at the temperature of the lake surface, and can be calculated from the temperature and the relative humidity.

Long-wave radiation emitted by the lake is calculated from the Stephan-Boltzman law,

$$Q_{lw} = -\epsilon k T_s^4$$

where k , is a constant ($5.67 \times 10^{-8} W m^{-1} \text{ } ^\circ K^{-4}$), ϵ is the emissivity (0.97 for water) and T_s is the surface temperature ($^\circ K$). The emitted radiation is partially emitted back towards the lake and reabsorbed together with long-wave radiation emitted by clouds. These two processes can also be introduced in the above formula,

$$Q_{wl}' = Q_{wl} (a - b P v^{1/2}) (1 - 0.6 C l^2)$$

where (a) and (b) are constants which vary from one geographical point to another, but in general they take values around 0.4 and

TABLE VI. Simulation results for the surface heat exchange for the ice-free period of 1984. *v*, wind speed ($m s^{-1}$); *t_s*, water surface temperature ($^{\circ}C$); *t_a*, air temperature ($^{\circ}C$); *Cl*, cloudiness (tenth of sky covered); *R_s*, incident radiation ($W m^{-2}$); *Q_o*, observed heat content change in the lake ($W m^{-2}$); *Q_s*, simulated heat content change in the lake ($W m^{-2}$); *hr*, relative humidity (%); *Q_s*, sensible heat flux ($W m^{-2}$); *Q_w*, heat exchange through evaporation ($W m^{-2}$); *Q_{lw'}*, long-wave radiation exchange ($W m^{-2}$). Suspect results are labelled with an asterisk (*). The model failed to adequately simulate the period near the thaw because it neglects the heat exchange through hydraulic input-output. *Simulación del intercambio superficial de calor para el período en que el lago estaba libre de hielo en 1984. v*, velocidad del viento ($m s^{-1}$); *t_s*, temperatura de la superficie del agua ($^{\circ}C$); *t_a*, temperatura del aire ($^{\circ}C$); *Cl*, nubosidad (décimas de cielo cubierto); *R_s*, radiación incidente ($W m^{-2}$); *Q_o*, cambio observado de contenido de calor en el lago ($W m^{-2}$); *Q_s*, cambio simulado de contenido de calor en el lago ($W m^{-2}$); *hr*, humedad relativa; *Q_s*, flujo de calor sensible ($W m^{-2}$); *Q_w*, intercambio de calor por evaporación ($W m^{-2}$); *Q_{lw'}*, intercambio de radiación de onda larga ($W m^{-2}$). Los resultados poco realistas se indican con un asterisco (*). El modelo falla en simular la fase cercana al deshielo debido a que no incluye el intercambio de calor por entrada y salida de agua.

Interval	Input Variables					Control		Simulated Variables			
	< <i>v</i> >	< <i>t_s</i> >	< <i>t_s</i> >	< <i>Cl</i> >	< <i>R_s</i> >	< <i>Q_o</i> >	< <i>Q_s</i> >	< <i>hr</i> >	< <i>Q_s</i> >	< <i>Q_w</i> >	< <i>Q_{lw'}</i> >
4-22 jul	4.0	6.1	15.2	0.3	302	199	305*	10*	205	-89*	-113*
- 12 aug	3.5	9.1	11.6	0.4	254	61	79*	10*	49	-103*	-121*
- 24 aug	3.5	9.9	12.3	0.4	230	122	128	50	47	-51	-99
- 3 sep	3.5	11.2	12.2	0.3	231	27	30	20	20	-106	-115
- 19 sep	3.2	10.7	9.0	0.6	172	-35	-34	50	-31	-66	-109
- 2 oct	3.3	8.6	5.6	0.5	138	-80	-77	60	-56	-55	-104
-17 oct	4.6	7.0	5.8	0.3	152	-62	-68	40	-31	-84	-105
-31 Oct	3.4	6.2	5.4	0.2	141	-12	-11	60	-15	-40	-96
-19 nov	3.5	5.0	1.7	0.7	67	-101	-118	100	-65	-19	-101
- 2 dic	3.5	3.4	0.7	0.3	78	-114	-114	60	-53	-40	-99

0.05, respectively (GILL, 1982; FREEPONG, 1983). *P_v* is the vapor pressure (mb) and *Cl* is the fraction of the sky covered by clouds, measured in a scale of 10.

The remaining heat exchange is produced by penetrative radiation of shorter wavelength (fig. 13). Therefore, availability of adequate meteorological data allows the calculation of heat changes in the lake (fig. 17). However, because the meteorological data available to us was incomplete, we used an approximation by means of a simulation model (table VI). The periods of time simulated corresponded to the intervals between subsequent visits to the lake. We used wind speed (*v*) values recorded at the Southern mouth of the Tunnel of Vielha. Sensibility to errors in these measurements are, however, small because its variability is relatively small. The mean surface water temperature (*t_s*) was approximated as the average temperature between subsequent visits. The average air temperature (*t_a*) was estimated from average maximum and minimum temperatures (CATALÁN, in press). Average cloudiness data (*Cl*) was

obtained from nearby Vaqueira meteorological observatory. The incident radiation was estimated as above, correcting the values by assuming an albedo of 0.03. The relative humidity (*hr*) was derived from the model to achieve agreement between the observed change of heat content (ΔQ_o) and the simulated mean heat flux (ΔQ_s). Therefore, the accuracy of the relative humidity used is critical for the performance of the model.

The calculated relative humidity tended to take values between 40 and 60% (table VI), that are similar to the average values recorded at the Vaqueira observatory for the same periods, and within the values recorded for other lakes. Significant deviations from these average values occurred for two periods (August 24 - September 4 and October 31 - November 19). The first anomaly corresponded to a persistent anticyclonic situation maintained to the end of August, 1984, and represented very low relative humidity (20%), whereas the second anomaly corresponded to the period with the maximum registered rainfall (fig. 8). These anomalous values, therefore,

appear coherent. Unfortunately, the values corresponding to the period comprised between thaw and the August 12 could not be accurately simulated. This limitation appears to be a consequence of the failure of the model to account for heat exchange due to the advective input and output of water and to the latent heat of fusion. The greater simulation error for the period subsequent to thaw, characterized by the presence of ice floes in the lake, is in agreement with this explanation. Advective heat exchanged was small (c. $1-2 \text{ W m}^{-2}$) for the rest of the remaining sampling intervals. Overall the simulated values appear sufficiently accurate to outline the main components of heat exchange throughout the ice-free period.

Thaw to mid August: The lake received high average solar radiation ($250-300 \text{ W m}^{-2}$) during this period. The lake experienced a net input of sensible heat both during the day (c. 200 W m^{-2}) and night (c. 50 W m^{-2}) up to late July, whereas nocturnal heat losses (c. -50 W m^{-2}) started in August. Evaporation losses were low (0 to 50 W m^{-2} in July and 20 to 80 in August) and varied according to the relative humidity.

- Second half of August: In this period, on average, thermal conduction and evaporation losses were balanced. The heat content of the lake continued to increase because of the penetrative radiation (c. 230 W m^{-2}) despite nocturnal heat losses duplicated (100 W m^{-2}).

- Transition from late August to September: This period of 1984 experienced an special situation of prolonged good dry weather, that offers some interesting comparisons with the previous period. The incident radiation received by the lake and the average air temperature were similar for the two periods. However, the lake gained fivefold more heat in the former than in the latter period. These differences are attributable to the increase in the surface temperature of the water that attenuated conductive heat exchange, and, particularly, increased evaporation, that doubled (c. -100

W m^{-2}) during this period to achieve values in the order of heat emission. The day/night contrast increased, in the night the loss by conduction reached 80 W m^{-2} , which together with the 150 lost through evaporation and emission, provoked an important nocturnal penetrative convection.

- September: The net heat exchange of the lake reached negative values. The incident radiation did not compensate for the conduction losses (the flux of heat remained negative during the night and a good fraction of the day), evaporation, and long-wave emission.

October: Due to favorable meteorological conditions incident radiation almost compensated for heat losses, although nocturnal heat loss remained high (270 to 350 W m^{-2}).

First fortnight of November: At this time, rainfall reached maximum values, such that relative humidity approached 100% and, consequently, evaporation was notably reduced (c. -20 W m^{-2}). The losses through conduction and emission exceeded the gain by radiation, that was reduced due to persistent cloudiness.

- Late November to early December: The situation of heat loss persisted during this period until lake freeze up. The daily flows ranged between -50 and -130 W m^{-2} and the nocturnal flows were of the order of -300 W m^{-2} .

Turbulent convection velocity associated to surface heat flux can be calculated, similarly to the calculations for wind action, from the expression,

$$C^* = (B h)^{1/3}$$

where $B = (\alpha g -Q) / (C_p \sigma_s)$ is the buoyancy flux, α is the thermal expansion, Q is the heat flux and h the depth of the upper layer

INFLOW AND OUTFLOW

Hydraulic inflow and outflow may be partially responsible for the modification of

the vertical structure of the lake. The main inlets of Lake Redó carry little water and can even dry up in summer, with a small and localized influence. In contrast, the effect of the outflow through the tube, that draws water from 4 m, could have greater importance. The effect could be evaluated through the calculation of a Froude number,

$$Fo = S / (H^2 (g' H) 1/2,$$

where S is the outflow, H the maximum depth, and $g' = g (\Delta\sigma/\sigma_s)$, where $\Delta\sigma$ refers to the difference between the surface density (σ_s) and that of the depth where the water is drawn out through the tube (IMBERGER & PATTERSON, 1981). Fo relates the inertial forces associated with the outflow with the gravitational forces associated to the vertical density gradients. Whenever $Fo > 1$ the inertial forces associated to the outflow exceed gravitational forces, and important horizontal gradients are formed. The denominator of Fo ranges, for Lake Redó from 60 to 180 $m^3 s^{-1}$. Evidently, water outflow never attains these values (average outflow c. 0.1 $m^3 s^{-1}$), so that $Fo \ll 1$.

The effect of water flow can also be characterized through the turbulent advective velocity,

$$R^* = (C_d V_s^2)^{1/2}$$

where C_d is the drag coefficient, with a similar magnitude to that used for the wind action, and V_s is the velocity of the water flow (CARMACK *et al.*, 1986). The maximum outflow velocity occurred during thaw and was about 0.1 $m s^{-1}$, so that in general for Lake Redó, $R^* < 0.0036 m s^{-2}$.

MIXING IN THE EPILIMNION

The relative importance of the factors discussed above upon mixing varies throughout the year. During the period of stratification we can compare them

assuming that the lake behaves like a two layer prismatic system, an upper layer (i.e., epilimnion) with a thickness h, and a lower layer (hypolimnion) with a thickness H-h. This approximation can be derived in different ways (PATTERSON *et al.*, 1984; CARMACK *et al.* 1986). We will take h to equal the depth where N^2 is maximum, and H equal to the mean depth (V/A) of the lake (32 m).

Although the epilimnion is not isotropic (IMBERGER, 1985), secondary thermoclines are never very important in Lake Redó and offer little resistance to the mixing induced from the surface. Similarly, the rotational effect of the Earth does not become manifest either because Rossby's radius always exceeds the lesser width of the lake.

SPIGEL & IMBERGER (1979) classified the dynamics of the mixing layer of small and medium lakes comparing the number of Richardson ($Ri = g' h / U^2$) of the two layers system with the morphological ratio L/h, where L is the effective length where the wind acts, and therefore, its maximum value is the length of the lake. They defined four types of mixing regimes:

Regime 1: $Ri < 1$. The basin is for all practical purposes homogeneous. Large displacements of the interface can occur, insofar as the concept of an interface is valid. Any longitudinal density differences remaining after vertical mixing will be incommensurable.

Regime 2: $1 < Ri < (L/2h)[H/(H-h)]^{1/2}$. Interface shear, Kelvin-Helmholtz billows, and rapid deepening accompany large interface displacements. Significant horizontal heterogeneity. The interface is unstable and loosely defined. Complete vertical mixing may occur during a single wind episode, resulting in a longitudinally stratified basin.

Regime 3: $(L/2h)[H/(H-h)]^{1/2} < Ri < (L^2/4h^2)[H/(H-h)]$. Internal seiching is the prominent feature of this regime. Buoyancy is strong enough that entrainment and billowing have minor effects on the density

determined constants, with the values 0.5, 0.13 and 1.23, respectively (FISHER *et al.*, 1979).

Entrainment of colder hypolimnetic water to the epilimnion involves cooling of the upper layer. The rate of cooling of the epilimnion is,

$$dT/dt = -Q / (C_p \sigma_s h) - \Delta T / h (dh/dt)$$

The first part of the term on the right of the expression refers to the temperature drop due to heat lost to the atmosphere and the second part refers to temperature drop due to entrainment of cold hypolimnetic water.

The evolution of the thermocline depth under specific wind and heat flux conditions is derived from the simultaneous solution of the two equations above. Their dynamic simulation can be achieved through the solution of the equations for successive time intervals, with the result of one iteration being incorporated into the next run.

As the introduction of energy depends on U^3 , averaging the data across different time intervals results in widely different results. For instance, a wind with a speed of 5 m s^{-1}

persisting during 24 h will introduce 16 times less energy than a wind of 20 m s^{-1} lasting only 6 h, even though the average wind intensity in a daily basis would be the same. Therefore, it is unlikely that the average estimates of C^* and U^* for the long time intervals between subsequent sampling dates permit accurate estimations of the observed changes in thermocline depth (dh). These calculations, however, permit the evaluation of the time scales and length of mixing for different water column situations, characterized through vertical temperature profiles, and the simulation of behavior of the mixing layer under different wind and heat flux combinations in short time intervals. We simulated periods of 4 hours calculated by intervals of 1 hour.

To analyze the mixing behavior of the lake we shall use the thermocline features, the temperature change in the epilimnion, the ratio h/q^* that represents the temporal scale necessary for a disturbance to mix the entire epilimnion, and $l_{mo} = U^{*3} / B$, the Monin-Obukov length that for positive heat fluxes indicates the depth where the mechanical effect associated with heating

HEAT FLUX $W m^{-2}$	WIND SPEED ms^{-1}												
	INITIAL				STABLE				DESTRUCTIVE				
	1.5	3.5	6.0	15	1.5	3.5	6.0	15	1.5	3.5	6.0	15	
1200	-	-	-	5	/	/	/	14	/	/	/	23	
600	-	-	42	5	/	/	12	/	/	/	21		
350	-	-	16	5	/	/	12	/	/	/	20		
200	-	○	14	5	-	-	12	/	/	220	20		
100	-	37	13	5	-	○	37	11	/	/	61	20	
50	-	25	12	5	-	-	31	11	-	-	53	20	
10	-	21	12	5	-	54	29	11	-	92	49	19	
-10	38	20	12	5	69	45	28	11	120	77	48	19	
-50	26	19	12	5	43	36	26	11	76	64	45	19	
-100	22	17	12	5	35	31	25	11	61	55	42	19	
-200	/	17	15	11	5	30	26	22	11	48	46	39	19
-350	/	15	13	10	5	23	22	20	11	40	39	35	19

FIG. 20. Calculated epilimnetic mixing times (min) under different heat fluxes and wind speeds. Three phases of the stratification period of 1984 are represented: initial (22nd July), stable (24th August) and destructive (19th September). Missing data represents combinations of heat flux and wind speed insufficient for complete epilimnetic mixing. The symbol (O) indicates the most common situation for the period and the dashed line delimits very unlikely situations. *Tiempo de mezcla del epilimnion (min) para distintas combinaciones de flujo de calor y velocidad del viento. Se presentan tres fases del periodo de estratificación de 1984: inicial (22 de julio), estable (24 de agosto) y destructiva (19 de septiembre). La falta de valores indica que con esa combinación de flujo de calor y velocidad del viento la mezcla del epilimnion no es posible. El símbolo (O) indica la situación más común para el periodo en cuestión y la línea discontinua delimita situaciones muy improbables para ese periodo.*

balances wind-induced mixing, and under net heat loss represents the depth below which penetrative convection is the most important turbulence component.

On the basis of water column structure (represented by N^2 , fig. 18) and the changes in the external forcing agents throughout the summer, epilimnetic mixing can be differentiated on three different periods: an initial phase, a phase of maximum stratification and a destructive phase. The mixing pattern characteristic of these three different periods can be illustrated by examining representative situations, corresponding to the conditions observed for July 22, August 24, and October 2 1984, respectively (fig. 20, 21, 22).

Initial phase: corresponds to the end of thaw period and a rapid water column stratification, characterized by a relatively shallow (4 a 6 m) thermocline. Because of the positive net daily heat flow the buoyancy of the upper layers increased in

relation to the lower ones. The water column was very stable during the moments of maximum daily heat input (c. 1200 W m^{-2}), such that a wind intensity $> 15 \text{ m s}^{-1}$ extended over an hour would be necessary to mix the whole epilimnion. However, because of the shallowness of the epilimnion a moderately strong wind (6 m s^{-1}) acting over an hour could achieve complete epilimnetic mixing during the moments of moderate (c. 600 W m^{-2}) heat input. Further, moderate winds (3.5 m s^{-1}) could deepen substantially the thermocline during the weak heat inputs ($< 100 \text{ W m}^{-2}$), characteristic of cloudy days and low solar angles. Moderately strong winds ($5\text{-}7 \text{ m s}^{-1}$) concurrent to small irradiances could deepen the thermocline very fast, about 2 cm h^{-1} (fig. 22). Such winds, although relatively rare, must have occurred frequently enough to be able to erode the thermocline down to 13 m in 15-20 days, thereby ending the initial phase. The water column change

		WIND SPEED m s^{-1}											
		INITIAL				STABLE				DESTRUCTIVE			
		h=6				h=14				h=24			
		1.5	3.5	6.0	15	1.5	3.5	6.0	15	1.5	3.5	6.0	15
HEAT FLUX W m^{-2}	1200	-3	-33	-165	>h	-2	-23	-117	>h	-3	-43	-217	>h
	600	-5	-66	-330	>h	-4	-46	-234	>h	-7	-26	-435	>h
	350	-9	-112	-566	>h	-6	-80	-401	>h	-12	-148	-745	>h
	200	-15	-197	>h	>h	-11	-139	-702	>h	-20	-259	-1304	>h
	100	-31	-393	>h	>h	-22	-279	>h	>h	-41	-518	>h	>h
	50	-62	>h	>h	>h	-44	-558	>h	>h	-82	-1036	>h	>h
	10	-310	>h	>h	>h	-219	>h	>h	>h	-408	>h	>h	>h
	-10	310	>h	>h	>h	219	>h	>h	>h	82	>h	>h	>h
	-50	62	>h	>h	>h	44	558	>h	>h	41	1036	>h	>h
	-100	31	393	>h	>h	22	279	>h	>h	20	518	>h	>h
	-200	15	197	>h	>h	11	139	702	>h	12	259	1304	>h
	-350	9	112	566	>h	6	80	401	>h	7	148	745	>h

FIG. 21. Calculated Monin-Obukov lengths (cm) for different heat flux and wind speed combinations. Three phases of the stratification period of 1984 are represented: initial phase (22on July), stable phase (24th August), and destructive phase (19th September). For positive heat fluxes, the calculated length represents the depth where the mechanical resistance associated to heating compensates for the wind-induced mixing, whereas the length indicates the depth below which the most important turbulence component is the penetrative convection whenever negative heat fluxes occur. The h symbol indicates those situations when the wind action impinges directly upon the thermocline. The most probable heat flux and wind speed combinations are indicated as in figure 21. *Valores de la longitud de Monin-Obukov (cm) para diferentes situaciones de flujo de calor y velocidad del viento. Se representan tres fases del periodo de estratificación: inicial, estable y destructiva. Para un valor positivo del flujo de calor, la longitud indica la profundidad donde el efecto mecánico asociado al calentamiento compensa la mezcla debida al viento. Para un valor negativo, la longitud indica la profundidad por debajo de la cual el componente de turbulencia más importante es la convección penetrativa. El símbolo h indica cuando la acción del viento actúa directamente sobre la termocline. Se indican las situaciones de flujo de calor y velocidad del viento más probables como en la figura 21.*

FIG. 22. Deepening of the interphase (cm) and change of the temperature difference between epilimnion and hypolimnion (10^{-2} °C) after different combinations of heat flux and wind speed lasting for 4 hours. Three phases of the stratification period of 1984 are represented: initial phase (July 22), stable phase (August 20), and destructive phase (September 19). *Incremento de la profundidad de la interfase (cm) y cambio de la diferencia de temperatura entre epilimnion e hipolimnion (10^{-2} °C) para diferentes situaciones de flujo de calor y velocidad del viento actuando durante 4 horas. Se representan tres fases del período de estratificación de 1984: inicial (22 de julio), estable (24 de agosto) y destructiva (19 de septiembre).*

		WIND SPEED $m s^{-1}$			
		INITIAL			
		$h=6\text{ m } \Delta t=3.43^{\circ}C$			
		1.5	3.5	6.0	15
1200		0 -69	0 -69	0 -69	116 86
600		0 -34	0 -34	0 -34	133 123
350		0 -20	0 -20	3 -14	141 153
200		0 -11	0 -11	5 -2	146 165
100		0 -6	0 -5	7 5	149 173
50		0 -3	1 -1	7 9	151 186
10		0 -1	1 2	8 13	153 189
-10		0 1	2 3	8 14	154 191
-50		1 4	2 7	9 17	155 195
-100		1 8	3 11	9 21	157 199
-200		3 16	4 19	11 29	161 207
-350		5 28	6 30	13 41	168 204
		STABLE			
		$h=14\text{ m } \Delta t=4.73^{\circ}C$			
		1.5	3.5	6.0	15
1200		0 -29	0 -29	0 -29	16 17
600		0 -15	0 -15	0 -14	23 49
350		0 -8	0 -8	0 -8	25 63
200		0 -5	0 -5	0 -5	27 71
100		0 -2	0 -2	1 0	28 77
50		0 -1	0 -1	1 3	29 79
10		0 0	0 1	2 5	29 82
-10		0 1	0 2	2 6	29 83
-50		1 3	1 4	2 8	30 85
-100		1 5	1 6	3 10	30 88
-200		2 11	2 12	4 16	31 93
-350		3 18	4 19	5 23	33 102
		DESTRUCTIVE			
		$h=24\text{ m } \Delta t=2.15^{\circ}C$			
		1.5	3.5	6.0	15
1200		0 -17	0 -17	0 -17	42 24
600		0 -8	0 -8	0 -8	57 54
350		0 -5	0 -5	0 -5	64 65
200		0 -3	0 -3	0 -3	68 56
100		0 -1	0 -1	2 1	72 66
50		0 1	0 1	3 3	73 68
10		0 1	1 1	4 4	74 69
-10		0 1	1 1	4 5	75 70
-50		1 3	2 3	5 6	76 72
-100		2 4	3 4	6 8	78 74
-200		4 8	5 8	8 11	81 78
-350		7 13	8 13	12 17	86 84

from the situation observed on July 22 to that recorded on August 12, represents an average thermocline deepening rate of 1.6 cm h^{-1} . Obviously, such fast deepening involved an important disturbance of the top of the hypolimnion, entraining hypolimnetic water to the epilimnion. A fairly strong wind ($> 13\text{ m s}^{-1}$) acting during periods of reduced radiation could mix the epilimnion in five minutes (Fig. 20a), and produce sufficiently fast enough subsidence and erosion of the thermocline through shear production to shift the water column to regime 2 conditions. Significant shear production, however, would not occur unless such winds lasted $>40\text{-}50$ minutes, the time necessary for the thermocline to slope (i.e., $1/4$ the oscillation period of the first internal seiche, $T_{si} = 2L / (g' h (H-h)/H)$). Because of the considerable water circulation through the lake at the beginning of the phase, the turbulence related to water outflow ($R^* = 3.6 \cdot 10^{-3}$) was similar to that produced by a moderate wind ($U^*(3.5\text{ m s}^{-1}) = 3.9 \cdot 10^{-3}$). During daily peak irradiance the buoyancy increase due to heating could probably be compensated before wind and advective mixing would reach the interphase. However, the combined effect of wind and advective mixing should result in enhanced thermocline deepening during reduced irradiance. R^* is not contemplated in the calculations of fig. 20, 21 and 22.

Maximum stability phase: Three factors cooperate to enhance the stability of the two layer system: (1) the greater epilimnetic temperature that results in the increased buoyancy of this layer, (2) the increased temperature difference between the epilimnion and hypolimnion that increased the energy necessary to mix them, and (3) the deeper interphase. Only the top meter of the epilimnion was mixed under normal ($1\text{-}4\text{ m s}^{-1}$) wind conditions during the day (fig. 21b), whereas mixing action could reach down to 7 or 8 meters under strong winds. Secondary diurnal stratification may develop, although this stratification

TABLE VIII. Hypolimnetic eddy diffusivity (K_z), and the contribution (%) of the received radiation to the temperature change observed at different depths. (A) From July 22 to August 24; (B) From August 12 to September 19; (C) From September 3 to October 2. Zero values are indicated whenever the sum of the measurement and calculation errors are of the same magnitude as the difference between the actual value and the molecular diffusivity of heat ($1.3 \times 10^{-7} \text{ m}^2 \text{ s}^{-1}$). *Coefficientes de difusividad turbulenta en el hipolimnion (K_z) y estimación de la contribución de la radiación al cambio de temperatura. A) Desde el 22 de julio hasta el 24 de agosto; B) Del 12 de Agosto al 19 de Septiembre; C) Del 3 de septiembre al 2 de Octubre. Los valores nulos indican que el error de medida más el de cálculo es del mismo orden que la diferencia entre el valor real y la difusión molecular del calor ($1.3 \times 10^{-7} \text{ m}^2 \text{ s}^{-1}$).*

m	z (10 ⁻⁶ m ² s ⁻¹)				% T			
	A	B	C	B	A	B	C	D
14	11	1.8	-	---	72	43	---	--
15	12	1.8	-	---	75	86	---	--
16	15	2.0	-	---	75	93	---	--
17	21	1.5	-	---	72	100	---	--
18	19	3.3	0	---	74	96	100	--
19	12	1.6	0	---	66	87	100	--
20	34	2.6	0	---	67	82	100	--
21	10	1.9	0	---	66	75	100	--
22	29	0.75	0	---	65	68	100	--
23	13	0	0	---	65	83	100	--
24	12	0	0	4.6	58	75	100	43
25	22	0	0	9.8	65	66	88	74
26	20	0	0	6.5	68	60	100	67
27	20	0	0	9.5	53	66	100	90
28	17	0	0	9.7	55	60	100	81
29	16	0	0	9.9	43	68	0	72
30	13	0	0	20	41	56	0	60
31	9.8	0	0	10	44	68	0	36
32	7.4	0	0	19	49	93	0	32
33	5.6	0	0	9.2	59	100	0	21
34	4.3	0	0	16	79	0	0	19
35	0	0	0	0	100	0	0	23
36	0	0	0	12	100	0	0	20
37	0	0	0	0	100	0	0	27
38	0	0	0	9	100	0	0	25
39	0	0	0	7.6	92	0	0	44
40	0	0	0	0	81	0	0	20
41	0	0	0	6.7	73	0	0	17
42	0	0	0	0	66	0	0	31
43	0	0	0	4.7	59	0	0	28
44	0	0	0	0	53	0	0	0
45	0	0	0	0	48	0	0	0

phenomenon would be quite ephemeral because wind intensities as low as 2 m s^{-1} could be sufficient to destroy any stratification within the first two meters, and because any stronger stratification would probably disappear overnight due to the negative heat fluxes (-200 or -250 W m^{-2}). Consequently, the epilimnion would probably be homogeneous by midnight (fig. 20b).

Since nocturnal penetrative convection had only a modest effect upon the vertical

stability of the seasonal thermocline, thermocline sinking was small (fig. 22 b). The stability phase lasted over a month in the year studied.

Destructive phase: The temperature difference between the epilimnion and the hypolimnion decreased as net daily heat fluxes reached negative values (towards the second fortnight of September), thereby increasing the vulnerability of the water column structure to wind action. Thermocline erosion eventually resulted in

greater thermocline sinking rates, although these events occurred always under regime 3 (table VIII). Consequently, the two-layer model remained valid until the interphase reached the bottom. In this period epilimnetic mixing could be attained within 0.5 and 2 h and there was continued turbulence acting upon the interphase. This was the 1984 period with stronger wind action. Wind intensities reached up to 15 m s^{-1} and could deepen the thermocline as fast as 25 cm h^{-1} . Thermocline loss considerably decreased the water column resistance to wind-induced mixing, such that weak wind intensities (c. 3.5 m s^{-1}) could result in complete vertical mixing in about 12 h. This indicates that the lake must have mixed completely several times a day.

MIXING IN THE HYPOLIMNION

Because convective and advective processes in the hypolimnion are relatively unimportant the flux-gradient method can be used to estimate diffusion (POWELL & JASSBY, 1974).

If K_z is the coefficient of vertical eddy diffusivity and Q_z represents the energy flux to a certain depth, then

$$Q_z = -\sigma c_p K_z dT_z/dz.$$

After applying the first law of thermodynamics and integrating from z to z_{\max} we reach the expression,

$$K_z = -1 / (\delta T_z / \delta z) (1/Az (d(\int Au Tu du)/dt) - (Rz / C_p \sigma))$$

where Az is the area over depth z and Rz the radiation reaching to depth z . The term Rz must be considered in transparent lakes like Estany Redó because it can account for a substantial fraction of the hypolimnetic temperature change. The fraction of the temperature change at any given depth, z , due to solar radiation can be estimated

through the following ratio (JASSBY & POWELL, 1975):

$$\delta(Az Rz) / \delta z / (c_p \sigma Az \delta T_z / \delta t)$$

There are several constraints to the application of this methodology to Lake Redó namely the few temperature profiles available, the slow temperature change in Lake Redó and the difficulties associated to the estimation of Rz . However, a compromise can be achieved by estimating K_z over extended periods of time (i.e., three consecutive visits or c. 1 month). We estimated Rz assuming that the hypolimnion received the direct component of the surface radiation alone, and assuming that 50% of that energy was efficiently absorbed through the epilimnion because its wavelength, and that the remaining energy declined according to $Rz = R_0 e^{-\mu z}$, where μ is estimated from the Secchi disk depth (POOLE & ATKINS, 1949). Although many of the values calculated lie within margins reported for other lakes (JASSBY & POWELL, 1975; IMBODEN *et al.*, 1983), the uncertainty involved in the calculations limit their accuracy, such that we will only discuss relative differences between the values obtained (table VIII). Hypolimnetic K_z values appear to be related to the lake area. Since Lake Redó has a similar size to Castle Lake, its K_z values should approach the average value $5 \times 10^6 \text{ m}^2 \text{ s}^{-1}$ reported for Castle Lake (JASSBY & POWELL, 1975). The different phases used to describe epilimnetic mixing appear to apply also to describe the seasonal variation of hypolimnetic diffusivity. The maximum K_z values were achieved at the initial phase (July 22 - August 24), when the thermocline deepened more quickly. The predictable association between the velocity of interphase deepening and hypolimnetic eddy diffusivity has been repeatedly documented (SWEERS, 1970). Hypolimnetic diffusivity decreased subsequently as the summer thermocline

tablished (August 12 - September 19). Hypolimnetic diffusivity was probably largely molecular ($1.3 \times 10^{-7} \text{ m}^2 \text{ s}^{-1}$) by the end of the phase (September 3). Hypolimnetic temperature increase during this period was mainly attributable to radiation (table VIII). Hypolimnetic diffusivity started to increase, probably achieving K_z values below those at the initial phase, after the interphase deepened more rapidly.

Hypolimnetic values attained their vertical maximum 5 to 8 m below the thermocline, and decreased with increasing depth to fall below the resolution of the procedure used. Vertical differences in K_z values were greater for high mean K_z values. Therefore, the vertical profile of K_z discriminates two layers within the hypolimnion: (1) an upper layer characterized by high eddy diffusivity and associated to thermocline dynamics, that extended from 15 to 30 m for most of the stratified period (August 12 - September 19) and that deepened (25-40 m) as the thermocline sunk; and (2) a bottom layer of smaller diffusivity composed of molecular diffusivity and, to a smaller extent, phenomena associated to boundary intrusions. The role of molecular diffusivity for some layers of stratified lakes has been previously reported (QUAY *et al.*, 1980).

MIXING UNDER ICE

The first ice generally forms overnight, when calm conditions are more probable. The entire lake surface can be covered by ice in a few hours given intense negative heat fluxes. The formation of the first ice cover impedes the mixing action exerted by the wind allowing ice formation to progress even if calm conditions disappear. However, the lake water experiences some degree of mixing due to the sediment heat loss. Convective motion under ice can also be prompted by radiation penetrating through the transparent ice during some

parts of the day, but reduced penetration due to accumulating snow soon reduces the importance of this process (CATALAN, in press). Other heat sources, such as geothermic heat (ALBERT & COROMINAS, 1985) or the heat produced during chemical oxidation (WETZEL, 1983) are irrelevant for Lake Redó

The influence of sediment heat loss is shown by the dynamics of the 3.5 isoline (fig. 14). The 3.5° C isoline sunk from lake freeze up to late February, when it stabilized at about 35 m. Evidence of mixing associated to boundaries has been provided by MORTIMER & MACKERETH (1958) for a Swedish lake, and has been confirmed more recently by WELCH & BERGMANN (1985). Welch and Bergmann (1985) used dyes and temperature and conductivity profiles to demonstrate the occurrence of this type of mixing for Canadian lakes with similar size as the Pyrenean lakes. It appears from the work of WELCH & BERGMANN (1985) that the water in contact with the ice cover moves laterally to sink close to shore. They postulate that upwelling of bottom waters must occur over the center of the lake to achieve mass conservation. LIKENS & RAGOTZKIE (1966) also described a horizontal, albeit rotational, water motion under ice, with cyclonic direction in the center of the lake and anti-cyclonic on the periphery. Although the nature of compensatory movements is not well understood to-date, there is consensus on the occurrence of downwelling associated to the boundaries. The scattered data available (LIKENS & RAGOTZKIE, 1965; WELCH & BERGMANN, 1985) agree in pointing out sediment induced convective velocities of the order of 10 m d^{-1} . This figure may be somewhat smaller for Lake Redó because the temperature drop of the water column during fall is not as important as that for Canadian and Arctic lakes. Whatever the exact current velocities under ice, the diffusion coefficient near the boundaries must be about $1 \times 10^{-3} \text{ m}^2 \text{ s}^{-1}$. Greater turbulence should be associated to

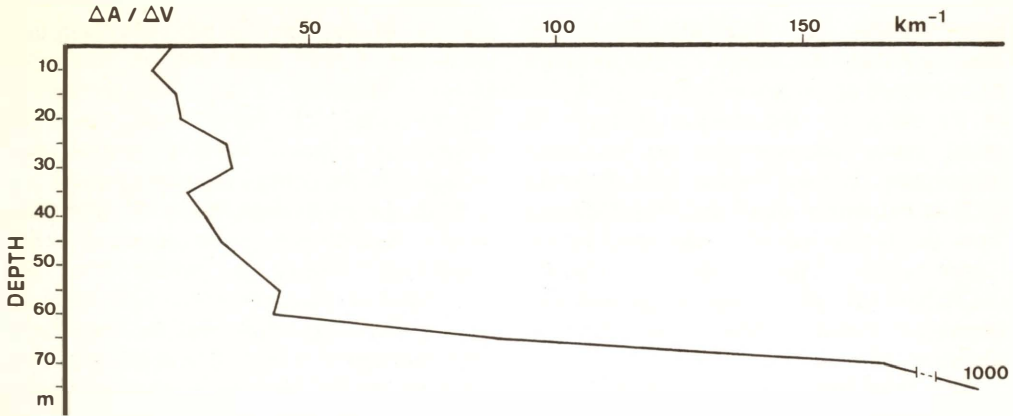


FIG. 23. Rate of change of area with respect to volume plotted against depth. *Cambio del área respecto del volumen en función de la profundidad.*

the layers with shallower slopes (fig. 23). Since the hypsographic curve of Lake Redó shows an inflection point at c. 40 m there must be a qualitative change in the turbulence of the water mass beneath this point before the sediment and the water reach a thermal equilibrium.

MIXING DURING THAW

Accumulated evidence (HILL, 1967; SCHINDLER *et al.*, 1974; HULBERG, 1977; BERGMANN & WELCH, 1985) indicate the water entering the lake during the thaw, while the lake is still covered with ice, circulates surficially towards the outlet without mixing with the lake water. Further, three water layers can be distinguished at certain moments: thaw water from the lake cover; thaw water from the basin; and lake water. Among these three water masses, that entering the lake from the basin has the shortest residence time. Differences in electric conductance can be used to discriminate the three surficial water masses in Lake Redó (CATALÁN, in press), although such differences are weaker than those reported for other lakes.

The extended duration of the ice cover permits the persistence of the stratified structure of the surficial water masses. This

causes the achievement of vertical isothermy to be achieved later and at greater water temperatures, and reduces the transit to summer stratification. The seasonal variation on the thickness of the snow and ice cover can be considerable: in 1984 the maximum thickness was 5 m whereas in 1985 it was only 2.5 m. The fusion of the ice finished 20 days earlier in the second year than in the first.

In the final phase of the thaw, when the lake surface is only partially ice-covered, there can be important horizontal temperature heterogeneity that induces surficial horizontal motion through gravitational adjustments. This aspect of horizontal heterogeneity is further enhanced by the wind-drift of ice blocks. The presence of gravitational instabilities are well represented in some vertical temperature profiles (fig. 18, July 4).

THE PHYSICAL ENVIRONMENT CONSTRAINTS TO THE BIOLOGY OF THE LAKE

The morphological characteristics of the lake and its basin are responsible for the oligotrophic nature of the lake. The external nutrient loading to the lake is scaled to catchment size (Ac) and, on the other hand, the received nutrients dilute in accord to the

lake volume (V). SCHINDLER (1971) suggested that these intuitive concepts could be combined on the use of their ratio (Ac/V) as an index of lake trophic status, with small ratios corresponding to increased oligotrophy. The Ac/V value for Lake Redó (0.2) is extremely small and, extrapolating from the results derived from lakes in the Experimental Lake Area of Canada (SCHINDLER, 1971) - also on granodiorite bedrock-, must result in extreme oligotrophy.

The importance of lake depth to the determination of their trophic status has long been recognized. In the 1920's THIENEMANN (1928) indicated that oligotrophy was related to lake depth, and RAWSON (1955) demonstrated an inverse relationship between mean depth and different measures of the lake production (dry weight of the plankton, dry weight of benthic fauna, fish production). More recently, UHLMANN (1985) attempted to explain this general pattern by arguing that the relationship between increased lake depth and oligotrophy relies on the reduced diffusion of deep lakes, greater sedimentation rates, smaller sediment areas above the hypolimnion, and limited sediment resuspension. In summary, increased depth represents a considerable dilution of recycled nutrients (MARGALEF, 1983). Since the external energy introduced by the processes of heat exchange and the mechanical action of the wind is the ultimate force responsible for the redistribution of recycled substances, the relation between the area of the lake, that defines the input window for such energy, and lake depth, the effective longitude to dissipate this energy, must play a primer role in the biological dynamics of the lake. This concept can be expressed in different forms, such as the relative depth (z_r), defined as the ratio between the maximum depth of the lake and the diameter of a circle with an area equal to the lake area. The value of z_r for the Lake Redó extraordinarily high (13%), compared to 7%

for one of the world's most oligotrophic lakes (i.e., Crater lake) and 3% for most lakes. Therefore, the morphometric characteristics of Lake Redó force a remarkable column stability despite the weakness of the density gradients formed.

With the expression $K_z = h^2 q^*/h$ the scale of mixing time can be estimated for an appropriate length h , which can be considered as the ratio between the volume over a particular depth and the lake area over that depth. The diffusion processes in the thermocline and the hypolimnion are negligible at the time scale of phytoplankton growth, although hypolimnetic intrusions through the thermocline occurring during thermocline sinking should have a bearing upon the seasonal evolution of biological productivity.

The sediment area over the hypolimnion varies throughout the year according to the deepening of the thermocline. Because of the hypsographic configuration of Lake Redó the water-sediment interaction should increase substantially above 40 m (fig. 23), and between 15 and 25 m, that corresponds to the Eastern sub-basin. Sediment resuspension should increase nutrient diffusion, particularly when mixing is exerted over flat bottoms, where the steep slopes of the lake should result in sediment focusing. We believe that sediment-water interactions must have an important role on the production peaks in Lake Redó.

Sediment resuspension should be greater in autumn than in spring. The duration and intensity of the spring mixing may be closely related to the duration and, therefore, the maximum thickness of the winter ice cover, so that we may expect summer productivity to be negatively correlated to winter precipitation.

Ambient temperature influences organismal physiology by influencing the thermodynamic and kinetic constants that determine the directions and speeds of chemical reactions (ALEXANDROV, 1977). According to HARRIS (1980a), the photosynthetic capacity of natural

phytoplankton populations relate to temperature as follows:

$$P_{\max} (\text{mg O}_2 \text{ mg Chla}^{-1} \text{ h}^{-1}) = 0.368 T (^{\circ}\text{C})^{1.23}$$

although this relationship is often confounded by the influence of other factors, specially nutrient concentrations (HARRIS, 1978). It seems there is no evidence of the existence of populations specially adapted to low temperatures, the epilimnetic and hypolimnetic temperatures of lake Redó probably set an upper limit to photosynthesis about 6 and 3.5 mg O₂ mg Chla⁻¹ h⁻¹ respectively, and about 2 mg O₂ mg Chla⁻¹ h⁻¹ during the mixing periods. These potential rates, however, may never be reached due to nutrient limitation.

Available data suggest a Q₁₀ for respiration in the order of 2-2.5 for the temperature range of Lake Redó (HARRIS, 1980). If respiration is expressed per unit chlorophyll, however, the value of Q₁₀ may be c. 1 because of the increase in chlorophyll and protein levels at low temperatures (HARRIS, 1978).

The photic zone is always deeper than the thermocline during the stratified period. Because a substantial fraction of the hypolimnion receives >1% of the surface irradiance photosynthesis may proceed in the hypolimnion and, therefore, there is no relationship between the thickness of the mixed layer and that of the photic zone. Epilimnetic phytoplankton is probably photoinhibited because irradiance may reach daily maxima of 200 $\mu\text{E m}^{-2} \text{ s}^{-1}$ near the

thermocline and because the radiation incident upon alpine lakes has a greater fraction of ultraviolet radiation (BLMANN *et al.*, 1987). Since epilimnetic mixing can be achieved in minutes to hours depending on the wind intensity, epilimnetic phytoplankton are probably exposed to photoinhibitory irradiances for a substantial fraction of the day. Thus, phytoplankton production may be photoinhibited, despite the ability of some phytoplankton species to adapt to high irradiances (CAPBLANCO, 1972; REYNOLDS, 1984). Even when the interphase is very deep or during the autumn mixing, the mixing time is within the time scale of the physiological response of phytoplankton (HARRIS, 1980b). Phytoplankton populations that are not adapted to high irradiances recruit to the epilimnion as thermocline sinks increasing the importance of photoinhibition. Even though phytoplankton residence time in the photoinhibition zone will be reduced, photoinhibition may occur upon exposure times > 5-10 minutes (REYNOLDS, 1984). The accumulation of snow in the surface of the lake reduces underwater irradiance to compensatory levels; phytoplanktonic populations, therefore, must incorporate heterotrophic organisms or minimize respiration to subsist (RHODE *et al.*, 1966). While the changes leading to winter darkness are somewhat gradual, spring ice crack is relatively fast, leading to a sudden radiation increase that must have a considerable influence on existing shade-adapted phytoplankton populations.

REFERENCES

- ADAMS, W.A. 1978. Effects of ice cover on the solar radiation regime in Canadian Lakes. *Verh. Int. Ver. Limnol.*, 16:321-332.
- ALBERT, J.F. & COROMINAS, J. 1985. La Geotèrnia. pp. 197-221. In: *Historia Nat. dels Països Catalans*, 3 (SERRAT, D., ed.): 197-221. Enciclopèdia Catalana. Barcelona.
- ALEXANDROV, V.Y. 1977. *Cells, molecules and temperature*. Springer Verlag, Berlin.
- BALLESTEROS, E. in preparation. Vegetació de la conca de l'estany Redó.
- BERGMANN, M.A. & WELCH, H.E. 1985. Spring meltwater mixing in small Arctic Lakes. *Can. J. Fish. Aquat. Sci.*, 42: 1789-1798.
- BIRGE, E.A. 1915. The heat budgets of American and European Lakes. *Trans. Wis. Acad. Sci. Arts. Lett.*, 18: 166-213.
- BOLSENGA, S.J. 1981. Radiation transmittance through lake ice in the 400-700 nm range. *J. Glaciol.*, 27(95): 57-66.

- BLMANN, B; BOSSARD, P & UEHLINGER, U. 1987. The influence of longwave ultraviolet radiation (u.v.-A) on the photosynthetic activity (14C-assimilation) of phytoplankton. *Journal of Plankton Research*, 9(5): 935-943.
- CAPBLANCO, J. 1972. Phytoplankton et productivité primaire de quelques lacs d'altitude dans les Pyrénées. *Annals Limnol.*, 8: 231-321.
- CARMARCK, E.C.; WIEGAND, R.C.; DALEY, R.I.; GRAY, C.B.I.; JASPER, S. & PHARO, C.H. 1986. Mechanisms influencing the circulation and distribution of water mass in a medium residence-time lake. *Limnol. Oceanogr.*, 31(2): 249-265.
- CATALÁN, J. 1986. Quan el Pirineu esdevé un laboratori. Anàlisi del projecte d'estudi limnològic de l'estany Redó. *Espais*, 2: 29-33.
- CATALÁN, J. (in press). The winter cover of a high-mountain mediterranean lake (Estany Redó Pyrenees). *Water Resources Research*.
- CHEN, C.T. & MILLERO, F.J. 1977. The use and misuse of pure water PVT properties for waters. *Nature*, 266: 707-708.
- CHOW, V.T. (Ed.) 1964. *Handbook of Applied Hydrology*. McGraw-Hill. New York.
- FISHER, H.B.; LIST, E.J.; KOH, R.C.; IMBERGER, J. & BROOKS, N.H. 1979. *Mixing in inland and coastal waters*. Academic Press. New York.
- FREEPONG, E. 1983. Diel aspects of the thermal structure and energy budget of a small English lake. *Freswat. Biol.*, 13: 89-102.
- GILL, A. E. 1982. *Atmosphere-Ocean Dynamics*. Academic Press. New York.
- GRACIA, C.A. 1983. *La clorofila en los encinares del Montseny. Interpretación como una optimización del aprovechamiento de la luz. Contribución a una teoría del árbol*. Ph. D. Thesis. Univ. Barcelona. Barcelona.
- HAKANSON, L. 1978. The length of closed geomorphic lines. *Mathematical Geology*, 10(2): 141-167.
- HAKANSON, L. 1981. *A Manual of Lake Morphology*. Springer. New York.
- HAKANSON, L. 1982. Bottom dynamics in lakes. *Hydrobiologia*, 91: 9-22.
- HARRIS, G.P. 1978. Photosynthesis, productivity and growth: The physiological ecology of phytoplankton. *Arch. Hydrobiol. Beih. Ergebn. Limnol.*, 10: 1-171.
- HARRIS, G.P. 1980a. The measurement of photosynthesis in natural populations of phytoplankton. In: *The physiological ecology of phytoplankton* (MORRIS, I., Ed.): 129-190. Blackwell. Oxford.
- HILL, H. 1967. A note on temperatures and water conditions beneath lake ice in Spring. *Limnol. Oceanogr.*, 12: 550-552.
- HARRIS, G.P. 1980b. Temporal and spatial scales in phytoplankton ecology. Mechanisms, methods, models, and management. *Can. J. Fish. Aquat. Sci.*, 37: 877-900.
- HULTBERG, H. 1977. Thermally stratified acid water in late winter - a key factor inducing self-accelerating processes which increase acidification. *Water Air Soil Pollut.*, 7: 279-294.
- HUTCHINSON, G.E. 1957. *A Treatise on Limnology*. Vol.1. Wiley. New York.
- IMBERGER, J. 1985a. The diurnal mixed layer. *Limnol. Oceanogr.*, 30(4): 737-770.
- IMBERGER, J. 1985b. Thermal characteristics of standing waters: an illustration of dynamic processes. *Hydrobiologia*, 125: 7-29.
- IMBERGER, J. & PARKER, G. 1985. Mixed layer dynamics in a lake exposed to a spatially variable wind field. *Limnol. Oceanogr.*, 30(3): 473-488.
- IMBERGER, J. & PATTERSON, J.C. 1981. A dynamic reservoir simulation model-DYRESM.5. In: *Transport models for inland and coastal waters*. (FISHER, H.B., Ed.): 310-350. Academic Press.
- IMBODEN, D.M.; LEMMIN, U., JOLLER, T. & SCHURTER, M. 1983. Mixing processes in lakes: mechanisms and ecological relevance. *Schweiz Z. Hydrol.*, 45(1): 11-44.
- JASSBY, A. & POWELL, T.M. 1975. Vertical patterns of eddy diffusion during stratification in Castle Lake, California. *Limnol. Oceanogr.*, 20: 530-543.
- KIRK, J.T.O. 1983. *Light and photosynthesis in aquatic ecosystems*. Cambridge University Press. Cambridge.
- LIKENS, G.E. & RAGOTZKIE, R.A. 1965. Vertical water motions in a small ice-covered lake. *J. Geophys. Res.*, 70: 2333-2344.
- LIKENS, G.E. & RAGOTZKIE, R.A. 1966. Rotary circulation of water in an ice-covered lake. *Vehr. Int. Ver. Limnol.*, 16: 126-133.
- MARGALEF, R. 1983. *Limnología*. Omega. Barcelona.
- MARGALEF, R.; CAMPAS, L; MIRACLE, M.R. & VILASECA, J.M. 1975. Introducción al estudio de los lagos pirenaicos. *Naturalia Hispanica*, 4: 1-47.
- MILLER, D.H. 1981. *Energy at the surface of the Earth. An introduction to the Energetics of Ecosystems*. Academic Press. New York.
- MORTIMER, C.H. 1974. Lake Hydrodynamics. *Mittl. Internat. Verein. Limnol.*, 20: 124-198.
- MORTIMER, C.H. & MACKERETH F.J.H. 1958. Convection and its consequences in ice-covered lakes. *Verh. Int. Ver. Limnol.*, 13: 923-932.
- PATTERSON, J.C.; HAMBLIN, P.F. & IMBERGER, J. 1984. Classification of the vertical density structure of lakes. *Limnol. Oceanogr.*, 29(4): 845-861.
- POOLE, H.H. & ATKINS, W.R.G. 1929. Photo-clectric measurements of submarine illumination throughout the year. *J. Mar. Biol. Assoc. U.K.*, 16: 297-324.
- POWELL, T.H. & JASSBY, A. 1974. The estimation of vertical eddy diffusivities below the thermocline in lakes. *Water Resour. Res.*, 10: 191-198.
- RAGOTZKIE, R.A. 1978. Heat Budgets of Lakes. In: *Lakes: Chemistry, Geology and Physics*. (IERMAN, A., Ed.): 1-19. Springer. New York.
- RAWSON, D.S. 1955. Morphometry as a dominant factor in the productivity of large lakes. *Verh. Int. Ver. Limnol.*, 12: 164-175.
- REYNOLDS, C.S. 1984. *The ecology of freshwater phytoplankton*. Cambridge University Press. Cambridge.
- RODHE, W.; HOBBIE, J.E. & WRIGHT, R.T. 1966. Phototrophy and heterotrophy in high mountain lakes. *Verh. Internat. Verein. Limnol.*, 16: 302-313.

- ROULET, N.T. & ADAMS, W.P. 1984. Illustration of the spatial variability of light entering a lake using an empirical model. *Hydrobiologia*, 109: 67-74.
- ROULET, N.T. & ADAMS, W.P. 1986. Spectral distribution of light under a subarctic winter lake cover. *Hydrobiologia*, 134: 89-95.
- RULL, V.; VEGAS, T. & NAVARRO, J. 1984. Extinción de la luz en los embalses españoles. Relaciones con la concentración de clorofila y las partículas en suspensión. *Oecologia aquatica*, 7: 25-36.
- SCHINDLER, D.W. 1971. A hypothesis to explain differences and similarities among lakes in the Experimental Lake Area, Northwestern Ontario. *J. Fish. Res. Bd. Canada*, 28: 295-301.
- SCHINDLER, D.W.; WELCH, H.E.; KALFF, J.; BRUNSKILL, G.J. & KRITSCH, N. 1974. Physical and chemical limnology of Char Lake, Cornwallis Island (75 N lat.). *J. Fish. Res. Bd. Canada*, 31: 585-607.
- SLY, P.G. 1978. Sedimentary Processes in lakes. In: *Lakes: Chemistry, Geology and Physics..* (LERMAN, A., Ed.): 65-89. Springer Verlag, New York.
- SPIGEL, R.H. & IMBERGER, J. 1980. The Classification of Mixed-Layer Dynamics in Lakes of Small to Medium Size. *Journal of Physical Oceanography*, 10: 1104-1120.
- SWEERS, H.E. 1970. Vertical diffusivity coefficient in a thermocline. *Limnol. Oceanogr.*, 15: 273-280.
- THIENEMANN, A. 1928. Der Sauerstoff im eutrophen und oligotrophen see. *Die Binnengewasser* 4, Schweizerbart. Stuttgart.
- VILAPLANA, J.M. 1983. *Estudi del glaciariisme quaternari de les altes valls de la Ribagorça*. Ph.D. Thesis. Univ. Barcelona. Barcelona.
- WELCH, H.E. & BERGMANN, M.A. 1985. Water circulation in small arctic lakes in winter. *Can. J. Fish. Aquat. Sci.*, 42: 506-520.
- WETZEL, R.G. 1983. *Limnology*. 2on ed. Sanders College. Philadelphia.
- WILLIAMS, G.P. 1971. Predicting the data of lake ice break-up. *Water Resources Research*, 6(1): 323-333.
- WOO, M. (Ed.) 1985. Hydrology of Snow and Ice. *The Canadian Geographer*, 29(2): 173-83.

